TRANSACTIONSNASTPHL
ISSN 0115-8848 (print)
ISSN 2815-2042 (online)
https://transactions.nast.ph/
Vol. 20 (1998)
doi.org/10.57043/transnastphl.1998.5833

Transactions NAST PHL, is the official journal of the National Academy of Science and Technology Philippines. It has traditionally published papers presented during the Academy's Annual Scientific Meeting since 1979 to promote science-based policy discussions of and recommendations on timely and relevant national issues as part of its functions as a national science academy. Starting in 2021, this journal has been open to contributions from the global scientific community in all fields of science and technology.

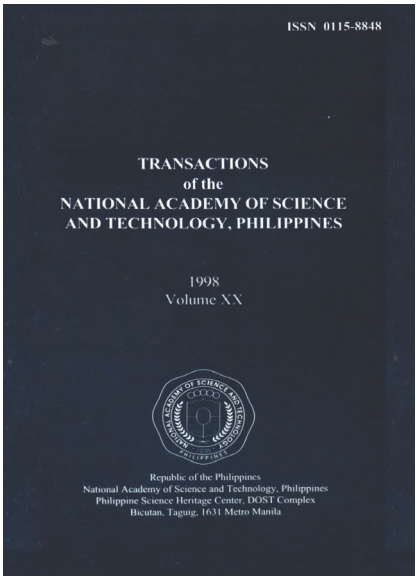

Growth, Emission and Excitation Spectra, and the Transition Pressures of $ZnSe_xS_{1-x}$ Single Crystals

Shirley Tiong-Palisoc

Department of Physics
De La Salle University
2401 Taft Avenue, Manila

Citation
Tiong-Palisoc S. 1998. Growth, emission and excitation spectra, and the transition pressures of $ZnSe_xS_{1-x}$ single crystals. Transactions NAST PHL 20: 427-466. doi.org/10.57043/transnastphl.1998.5833

GROWTH, EMISSION AND EXCITATION SPECTRA, AND THE TRANSITION PRESSURES OF $ZnSe_xS_{1-x}$ SINGLE CRYSTALS

SHIRLEY TIONG-PALISOC, Ph.D.
Department of Physics
De La Salle University
2401 Taft Avenue, Manila

ABSTRACT

$ZnSe_xSe_{1-x}$ single crystals which can be used in blue luminescent devices are prepared by sublimation method and their crystal structure is confirmed to be zincblende from x-ray diffraction analysis and the crystal composition x is determined from the lattice constant assuming Vegard's law holds for the $ZnSe_xS_{1-x}$ crystal system.

The photoluminescence spectra of the crystals are measured. Free exciton luminescence are detected. Bound exciton emissions are very pronounced indicating the presence of substitutional impurities in the form of neutral donors and acceptors. The incorporation of Na or Li is observed to enhance donor-acceptor pair transitions where the DAP band of the Li-doped sample. The energies of the luminescence transitions decrease curvilinearly with the increasing ZnSe composition x ($0.80 \leq x \leq 1$). The binding energies of the Al donor and the Na acceptor of $ZnSe_{0.94}S_{0.06}$ are 25.5 and 122.6 me V, respectively. The energies of the optical phonons LO and TO for the aforementioned crystals are 31.3 and 26.4 MeV, respectively. These energies are determined by excitation spectroscopy.

The statistic phase transition points of ZnSe and $ZnSe_xS_{1-x}$ ($0.40 \leq x \leq 1$) sing crystals in the high pressure region are also determined based on the transformation pressures region are also determined based on the transformation pressures of Bi I-II, Bi III-V and ZnS using the cubic anvil method where the pressure-induced variation of resistance is measured. The transition pressures of the samples vary linearly with the composition of ZnS in $ZnSe_xS_{1-x}$

The shock compression curves of $ZnSe_{0.85}S_{0.15}$ single crystals are also investigated. The pressure-particle velocity Hugoniot is found to agree with the corresponding Hugoniots of ZnS and ZnSe up to the phase transition point. The P-V isotherm of $ZnSe_{0.85}S_{0.15}$ derived from the U_s-u_p Hugoniot is consistent with the calculated P-V curve based on Bridgman's static data of ZnS and ZnSe.

I. INTRODUCTION

Considerable attention has been paid to the evaluation of the fundamental properties of the II-VI semiconductors and their application in devices. To date, the material quality of these semiconductors remains inferior to that of Si and III-V semiconductors. However, in spectral regions where Si and III-V devices cannot provide the required bandgap, the II-VI semiconductors are of potential importance in optoelectronic devices such as short wavelength (visible) light-emitting diodes, electroluminescent panels, optical waveguides, and photovoltaic solar cells. Recently, major efforts have been devoted to realizing visible light-emitting devices from the green to near-uv region with the wide bandgap Zn-chalcogenides[1]. The Zn-chalcogenides have a direct wide energy bandgap between 2.25 and 3.76 eV. There is an efficient direct band-to-band recombination in these materials, which implies that efficient light-emitting devices can be expected with effective injection of minority carries. ZnSe and ZnS are especially important for blue light-emitting devices[1] since the near-bandgap emission of ZnSe occurs at 460 nm and that of ZnS at 340 nm. However, control and understanding of intrinsic doping in such bulk II-VI compounds is far from complete. For example, the degree of control of conductivity has been hampered by the self-compensation effect[2,3] and the residual impurities in these materials which cause difficulties in fabricating low-resistivity p-n junctions – a prerequisite for efficient minority carrier injection devices. While the interpretation of the compensation effect is still contentious, the electrical and photoluminescence properties can be controlled effectively by intentional impurity doping.

The choice of ZnSe and $ZnSe_xS_{1-x}$ in this study as examples of wide bandgap energy (E_g) II-VI semiconductors is rationalized by the fact that they possess large enough E_g to yield blue light-emitting diodes. Addition of sulfur to ZnSe results in a ternary alloy with a higher bandgap, fulfilling a requirement needed to fabricate heterostructure devices.

To identify the role of various extrinsic impurities and intrinsic defects in the optical and electrical properties of these compounds, emphasis has been placed on the growth of purer bulk single crystals. With purer crystals, the concentration of background impurities is limited. The reduction of background impurities makes possible the identification of the role of donors and acceptors in these compounds. This effort suggests strongly that amphoteric doping can be possible by: (i) controlling the background impurities and (ii) enhancing the incorporation of appropriate dopants.

The high pressure polymorph of ZnSe and ZnS is also of considerable interest. Notwithstanding their wide bandgaps, they undergo a semiconductor to metallic phase change characterized by a fall in electrical resistance and a transition to a more closely packed structure. Their pressure-induced phase transition points are among those that make up the fixed-point static calibration curve[4-8]. Most of the reported studies are directed toward the measurement of the static

transformation pressure. However, there is substantial disagreement in the magnitude of the transformation pressures for ZnSe and ZnS. The experimental results are from different measurement methods and the pressure versus applied load scales are revised several times. It will be quite noteworthy if the transition points of ZnSe, ZnS and $ZnSe_xS_{1-x}$ are measured by the same method statistically and compared with dynamical results as obtained from shock wave loading.

This study aims to investigate, analyze, and present the growth, emission and excitation spectra, and the transition pressures of $ZnSe_xS_{1-x}$ single crystals. Specifically, the author seeks to discuss exhaustively the preparation of $ZenSe_xS_{1-x}$ single crystals and its growth by means of the self-closed sublimation method; investigate the x-ray diffraction pattern of the grown crystals and confirm that the lattice constants vary linearly with the composition of $ZnSe_xS_{1-x}$ according to Vegard's law after crystallization; at 4.2 K, measure and analyze the near-band edge emission spectra of $ZnSe_xS_{1-x}$; characterize the donor-acceptor pair transitions of the single crystals by evaluating their excitation spectra; report the pressure-induced static phase transformation points of $ZnSe_xS_{1-x}$ using the resistance variation method; and present the Hugoniot curves of $ZnSe_{0.85}S_{0.15}$ derived by means of shock wave loading.

Review of Related Literature

The first detailed studies of shallow acceptors in ZnSe using pair-spectral analysis was performed by Dean and Merz[9] in ZnSe. They observed two pair bands R_0 and Q_0, respectively, at liquid helium temperature. The high energy peaks R_0 at 2.708 eV and Q_0 at 2.692 eV were observe at moderately high excitation intensity. Both showed pairlike behavior but only R_0 was claimed to have discrete pair lines associated with it. Furthermore, only one free-electron to bound-hole transition (FB) associated with the Q_0 peak was observed at high temperature (60K) . From the analysis of the discrete pair lines, the value $E_A + E_D$ = 141 meV was obtained. Individual impurities responsible for these specific donor and acceptor were not known; however, both were located at the same sublattice. Merz et al.[10] later analyzed several samples of purposely doped ZnSe with Li and its isotope. They established beyond doubt that the lethium acceptor was indeed responsible for the pair band Q_0, and gave rise to discrete pair lines when codoped with Ga, In, and Al donors. The value of $E_A + E_D$ derived was 141 $\pm$ 2 meV. Since the donor binding energies had already been determined by Merz and co-workers[10] the Li-acceptor level was derived as 114 $\pm$ 2 meV. Merz et al.[10] also claimed that the Li acceptor was responsible for the pair lines observed by Dean and Merz[9] and that the R_0 pair band did not produce any pair lines. Dean[11], however, provided an alternative explanation which claimed that the R_0 peak is due to a deeper donor than shallow group III donors and a shallower acceptor than Liz_n is involved. The acceptor or donor could even be an axial one.

Ryal and Allen[12] ascribed the blue electroluminescence in Schottky diodes to the free exciton recombination by comparing the energy of the emission peak

with the free exciton energy reported by Hite et al.[13].

Bouley et al.[14] attributed the blue photoluminescence in Al- and Ga-doped ZnSe at room temperature to an overlap between the exciton and band-to-band transitions by extrapolating the low temperature free exciton energy by Hite et al.[13] to room temperature.

Yamaguchi et al.[15] who observed the temperature dependence of the blue electrolluminescence in ZnSe MIS diodes at 80 to 300 K proposed a transition due to the recombination of excitons bound to neutral donors.

Fujita et al.[16] also have analyzed the spectral shape of the room temperature blue photoluminescence in ZnSe layers grown epitaxially from a Zn-Ga solution and have proposed the band-to-band transition.

Chatterjee et al.[17] studied ZnSe samples which were fired in molten zinc either with Na or Al. In Na-doped samples, they observed two pair bands at 4.2 K peaking at 2.695 and 2.680 eV, respectively.

Rosa and Streetman[17] studied the ion-implanted ZnSe samples observed a pair peak at 2.701 eV as estimated. This peak was seen in Na-implanted samples which were all appropriately annealed around 600°C. They attributed this pair band peak at 2.701 eV to the Na acceptor. They further analyzed the temperature dependence and shift of the pair peak with excitation intensity and they concluded that the peak at 2.701 eV was indeed due to a donor-acceptor transition. The acceptor responsible for this particular band was assigned as Na on the basis of mass spectrographic analysis and absorption-impurity analysis. They presented quite convincing arguments to associate the peak at 2.701 eV with Na.

Gezci and Woods[19] studied the pair bands in ZnSe and observed three bands with zero-phonon peak energies at 2.678 eV, 2686 eV, and 2.705 eV. Pair lines associated with any of these bands were not detected but all three showed shifts to higher energy when excitation was increased. The bands at 2.678 and 2.686 eV were observed in crystals annealed in Zn atmosphere and bands at 2.678 and 2.705 eV were seen in crystals grown in excess selenium. Comparing these results to studies of Bryant et al.[20], they tentatively assigned the 2.686- and 2.705-eV bands to the same acceptor and donor but associated with random and preferential pairing. They assigned the binding energies of acceptors responsible for the 2.686- and 2.678-eV bands as 112 and 122 meV, respectively.

Swaminathan and Green[21] studied in detail the pair emission in melt-grown ZnSe. They observed five different pair recombination bands at 4.2 K with zero-phonon peak energies at 2.715, 2.702, 2.698, and 2.680 eV. The pair bands at 2.680 and 2.691 eV were associated with Alz_n-Liz_n donor-acceptor pairs, respectively.

Gross et al.[22] carried out the first detailed study of the shape of the zero-LO phonon emission line together with its one-LO and two LO phonon replicas over a range of temperatures. This led to a theoretical consideration of the-LO phonon-assisted emission spectra by Segall and Mahan[23] using a weak coupling approximation for both the exciton-photon and exciton-phonon interactions and by Tait

and Weiher[24] using the approximations of weak coupling between polaritons and phonons. Segall and Mahan[23] calculated the effect of LO phonon coupling on the width of the zero-LO phonon line.

Ohmori et al.[25] observed at 10K, the near-bandedge emission spectrum for melt-grown zinc-sulfo-selenide single crystals fired in molten zinc. It was found in this work that the bandgap obtained from the emission peak due to the excitonic transition near the bandedge varies monotonic curvilinearly with the composition of $ZnSe_xS_{1-x}$.

Ohishi[26] reported the time-resolved studies on recombination luminescence of donor-acceptor pairs in ZnSe. The binding energy of the Al donor was determined to be 26.7 meV and that of the Na acceptor was 114 meV. It was also confirmed that the hydrogenic model for energy levels as well as the Bohr radius apply for the Al donor. On the other hand, for the Na acceptor the Bohr radius which satisfied the experimental decay kinetics should be less than half of the value calculated using the effective-mass calculation.

Aside from their optical properties, ZnSe and ZnS have been studied at very high pressures and both have been found to undergo phase changes. The pressure-induced phase changes of these semiconductors are of much interest because they are among the transitions that make up the fixed-point static calibration curve[27].

The pressure versus applied load curve was initially proposed by Balchan and Drickamer[4] in 1961. They used a high pressure electrical resistance cell and the calibration was based on the barium transition at 5.9 GPa, the bismuth transition at 9.0 GPa and an extrapolation of Bridgman's data. The scale was revised downwards in 1970 by Dricknamer[5] changing the transition pressure for ZnSe from 18.0 to about 15.0 GPa and that for ZnS from 24.0 to 18.5 GPa where the calibration was based mainly on x-ray diffraction work.

Piermarini and Block[6] reported the static transition pressure for ZnSe as 13.7 GPa and for ZnS as 15.0 GPa. They utilized the diamond anvil type optical cell and measured pressure by means of the ruby fluorescence technique. They found that the revised 1970 fixed point scale and the ruby (NaCl) scale diverge above 13.5 GPa and differed by as much as a factor of 2 in the 50.0 GPa range.

Le Niendre et al.[7] employed pressure-induced variation of electrical resistance to determine the transition in ZnS and found that the transition to a conducting state occurred at 15.0 GPa.

Yagi and Akimoto[28] reported the transformation pressure of ZnS to be 16.2 GPa which was measured by means of an x-ray diffraction technique using NaCl as an internal pressure standard based on Decker's equation of state[29] for NaCl.

W.H. Gust[27], on the hand, utilized shock wave loading technique and determined the phase transition stresses to be 14.6 GPa for ZnSe and 17.4 GPa for ZnS.

II. GROWTH OF $ZnSe_xS_{1-x}$ SINGLE CRYSTALS

Crystals of very high quality have been made by vapor methods[30,31], but the rates of growth have been frustratingly low. In addition, the rate of growth seems to decrease with time. The lower temperatures involved favor high perfection, especially with those compounds which have a phase transition below the melting point, such as ZnS and ZnSe. The congruent nature of the evaporation in the case of these compounds makes vapor growth feasible.

It is a common experimental observation that during a phase transformation leading to crystal growth, the phase will not appear when the system reaches the thermodynamical phase boundary (saturation) but only when it becomes supersaturated. The theoretical explanation of the necessity of supersaturation for nucleation was given first by Gibbs[32] – the energy needed for the formation of the surface of the nuclei of the new phase is very important for the nucleation. This energy can be acquired by the system not at the equilibrium state (T=0) but only in an undercooled state.

For the growth of the single crystals in evacuated self-closed quartz ampoules from the vapor phase, undercritical supercooling is used to allow only selective nucleation on a small number of sites on the walls; a tapered ampoule tip is also used to localize nucleation and promote the formation of large single crystals at the tip of the ampoule. With the assumption of a statistical distribution of imperfections and impurities on the quartz walls, the area where onset of nucleation takes place should be kept as small as possible. The most convenient form to achieve this is by tapering one end of an ampoule which is placed through a temperature gradient. Since Pizzarello[33] used a tapered ampoule for crystal growth, several investigators have used this method more or less successfully and were able to grow massive single crystals. Piper and Polich[34] modified the system of Reynolds[35] and used the tapered ampoule geometry with much more complicated horizontal arrangement and a selfsealing ampoule. This approach however, did not offer any advantage in comparison with the simple vertical ampoule of Pizzarello[33]. Although this fact is well accepted now, the name of Piper and Polich[34] is still often mentioned in conjunction with Pizzarello's ampoule geometry. In this study, the horizontal method is used. The drawback of the vertical arrangement is that some thermal convective flow can take place in the furnace tube. As convective flows are not stable, this could give rise to small variations of the temperature profile around the ampoule.

The question of the actual supercooling in the ampoule arises. In general, it suffices to measure the temperature profile along the axis of the heating tube (without the ampoule in it) and to operate with the apparent supercooling given by this profile. For more exact measurements, however, an ampoule with an attached differential thermocouple can be used.

The thermal instability of recrystallization and low compatibility of quartz at higher temperatures are to be considered. It is well known, however, that there is a

great need for single crystals with high melting point. Several of these compounds can be grown from the melt and a few by flux techniques. Many others have melting points higher than those which can be mastered successfully in growth from the melt, or melt peritectically, decompose, or undergo undesirable phase transitions at very high temperatures. For such compounds, crystal growth from the vapor phase is very desirable.

Growth in a closed system in an atmosphere of their own vapor (sublimation) is in principle suitable for the growth of compounds with stoichiometric composition. However, deviations from stoichiometry are often encountered in compounds whose crystals are grown at high temperatures, as a preliminary to partial decomposition. Very often, such deviations from stoichiometry can be traced by changes in the physical properties of the compound. The same is true for contamination, reducing purity. For this reason, most of the crystals grown by high-temperature vapor growth have been intensively characterized by chemical, physical, and crystallographic methods.

It is to be noted that the more one is concerned with the problem of purity, the more relative it appears. Clearly, any data on purity must consider all the elements of the periodic system as possible impurities. Growth by sublimation is, obviously free from incorporation of transporting agent. In general, crystals grown by high temperature vapor growth methods are rather pure provided that pure starting materials can be used. Contamination from crucibles and handling atmospheres can be kept very low even at these high temperatures. Additional purification can be achieved by segregation effects which accompany the solid-vapor-solid transformation involved in the crystal growth process. Quartz ampoules are used which limit the growth temperature to 1250°C. The use of quartz at high temperatures may result not only in the contamination from the quartz, but also in the rapid diffusion of contaminants from the furnace refractories through the quartz. Because of their simplicity of fabrication and operation, sealed quartz ampoules have been the most popular. However, in this work, ampoules which are partially open for at least the beginning of the growth are used because they offer a remarkable advantage. The use of an open-necked ampoule can rid the starting material of volatile impurities before growth.

ZnSe and ZnS powder, both of 6-nine purity are used for the preparation of the $ZnSe_xS_{1-x}$ starting material in powder form. With mole proportions of ZnSe and ZnS calculated, samples of both materials are measured and thoroughly mixed and packed in a quartz tube the axial center of which is made hollow to allow gas flow. After packing, the sample container is inserted in a translucent quartz tube (45 mm-diam, 150 cm long) which is heated in an electric furnace at 1000°C with a stream of hydrogen gas for 1 hr. The sample is taken out and pound after the sample container is removed from the furnace. The starting material (in powder form) is then ready for crystal growth.

A transparent quartz tube (10 mm-diam, about 37 cm long) is heated and tapered reducing the diameter of the part which is 7 cm from one end to about 1 to 2 mm; after which, a small quantity (about 20 g) of the starting material is placed inside the tube. The prepared growth tube (container and sample) is set in a translucent quartz tube (45 mm-diam, 150 cm long) which is then inserted in a precision tubular electric furnace (Shimadzu Konzoku). The growth tube is set in such a way that the neck is 7 cm from one edge of the electric furnace which is the location of recrystallization temperature as shown in Fig. 1.

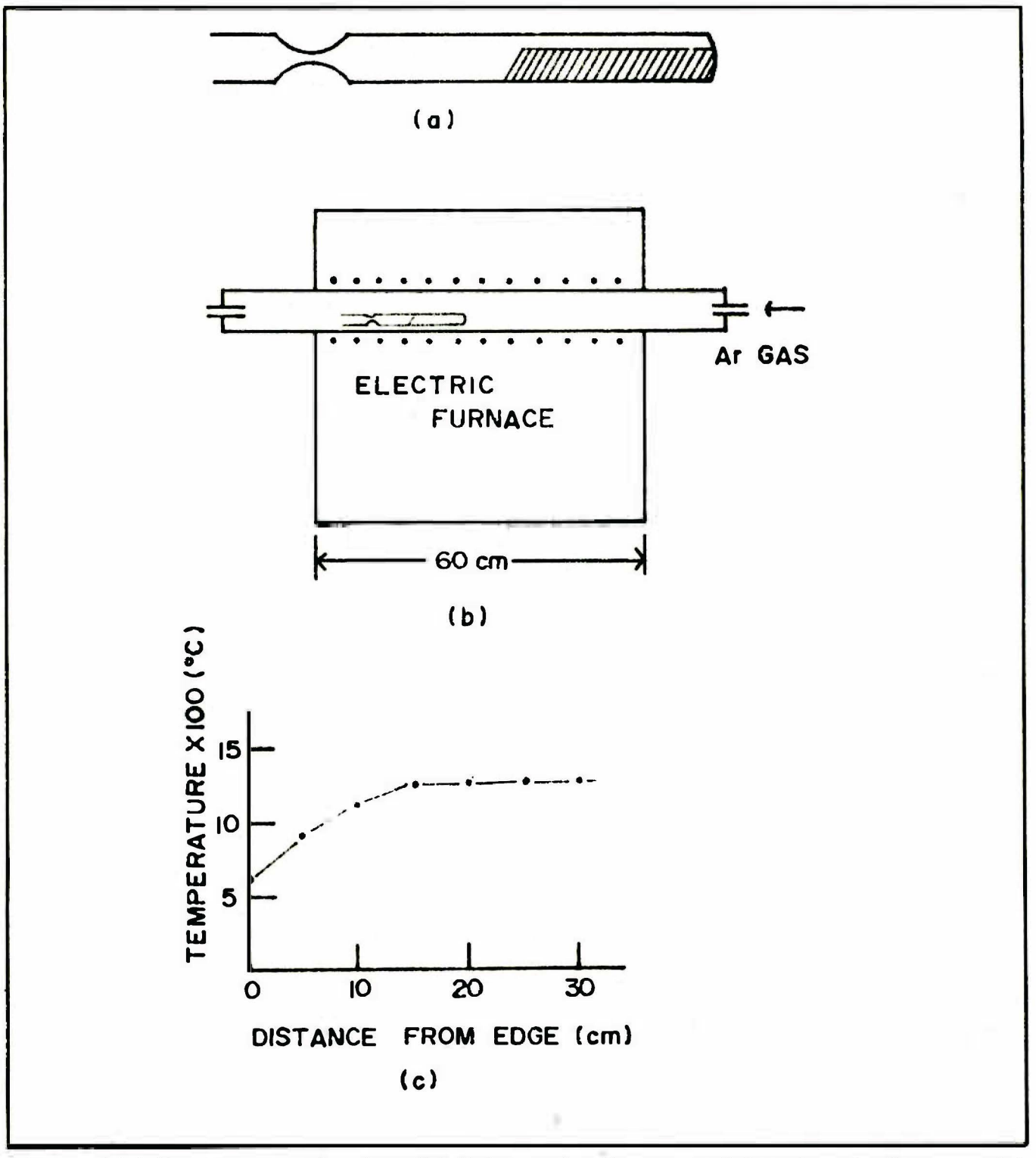

Figure 1(a) Quartz growth tube, (b) Schematic diagram of the electric furnace, (c) Temperature distribution of the furnace.

Prior tot he actual growing procedure of the sample, the translucent quartz tube is evacuated by means of a rotary oil pump until the pressure has become lower than 10^{-3} torr. Argon gas is then replaced twice and finally, it is allowed to flow at a rate of 0.1 li/min; henceforth, after 24 hr, the electric furnace is set to operate. The crystals are then grown from the starting material from 3 to 7 days by means of the sublimation method in a self-closed way at 1250°C in a stream of Ar gas at a flow rate of 0.1 li/min. Argon gas is used to prevent oxidation of the growth crystal. It is to be noted that the crystals are grown separately according to their composition.

Evaluation of the Grown Crystals

There are up to about ten ingots of crystals per growth cycle. The average size of each ingot is about 0.5 mm^3. Some of the crystals grown have well-cleaved planes and almost all are facetted with no twins. Figure 2 shows a photograph of grown ZnSe. The well-developed planes are the (111) and (110) planes as determined from the Laue diffraction patterns of $ZnSe_{0.95}S_{0.05}$ [(111) plane] as shown in Fig. 3 and $ZnSe_{0.92}S_{0.08}$ [(110) plane] as shown in Fig. 4.

It is interesting to note that when ternary compound crystals of ZnSexS1-x are grown, satisfactory results are obtained for selenium-rich crystals with x70.7. With increasing sulfur content (values of x<0.7) agglomeration of dendritic needles are formed in the first run and the morphology of the crystals is very similar to that of pure ZnS. Since the crystals are assumed to have been formed in the initial stages, they are subjected to another growth cycle. In the second run, the crystals are well-formed. No intermediate stage is observed with the ternary compound crystals. This suggests that the facets found on the ZnSe crystals are attributable to growth rate rather than condensation limitation.

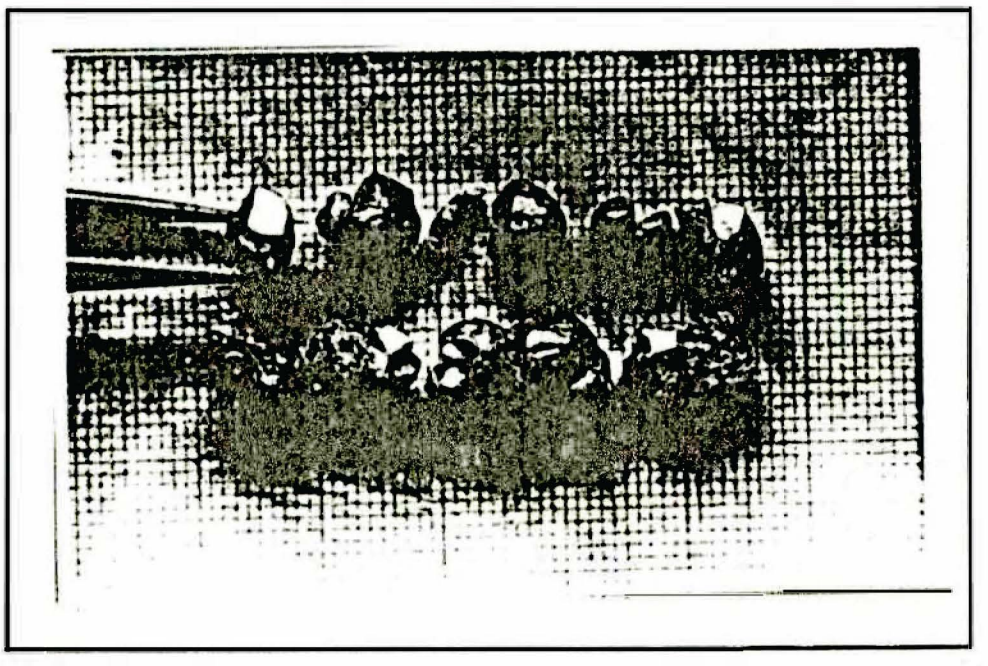

Figure 2. Sample crystal photograph of ZnSe grown in one growth cycle.

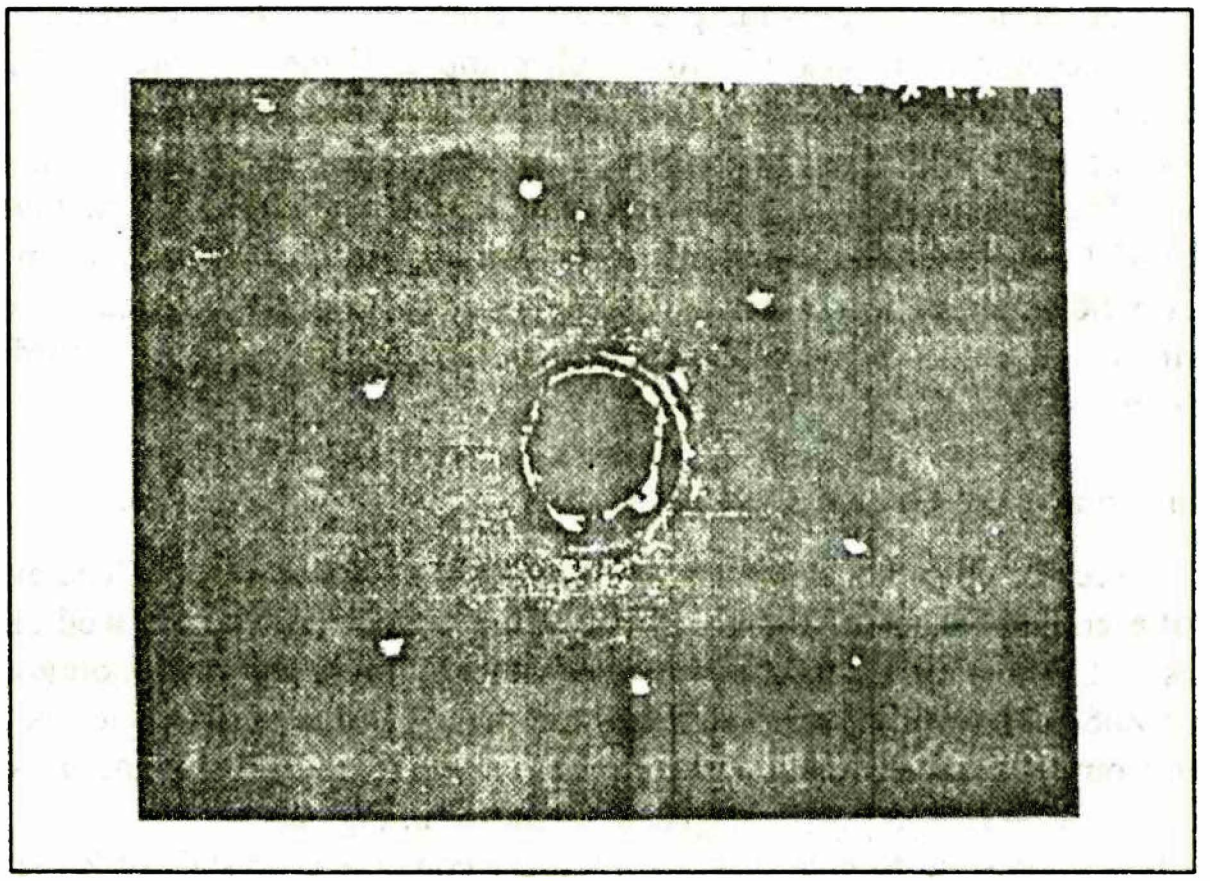

Figure 3. Laue diffraction pattern of the well-developed (111) plane of $ZnSe_{0.95}S_{0.05}$

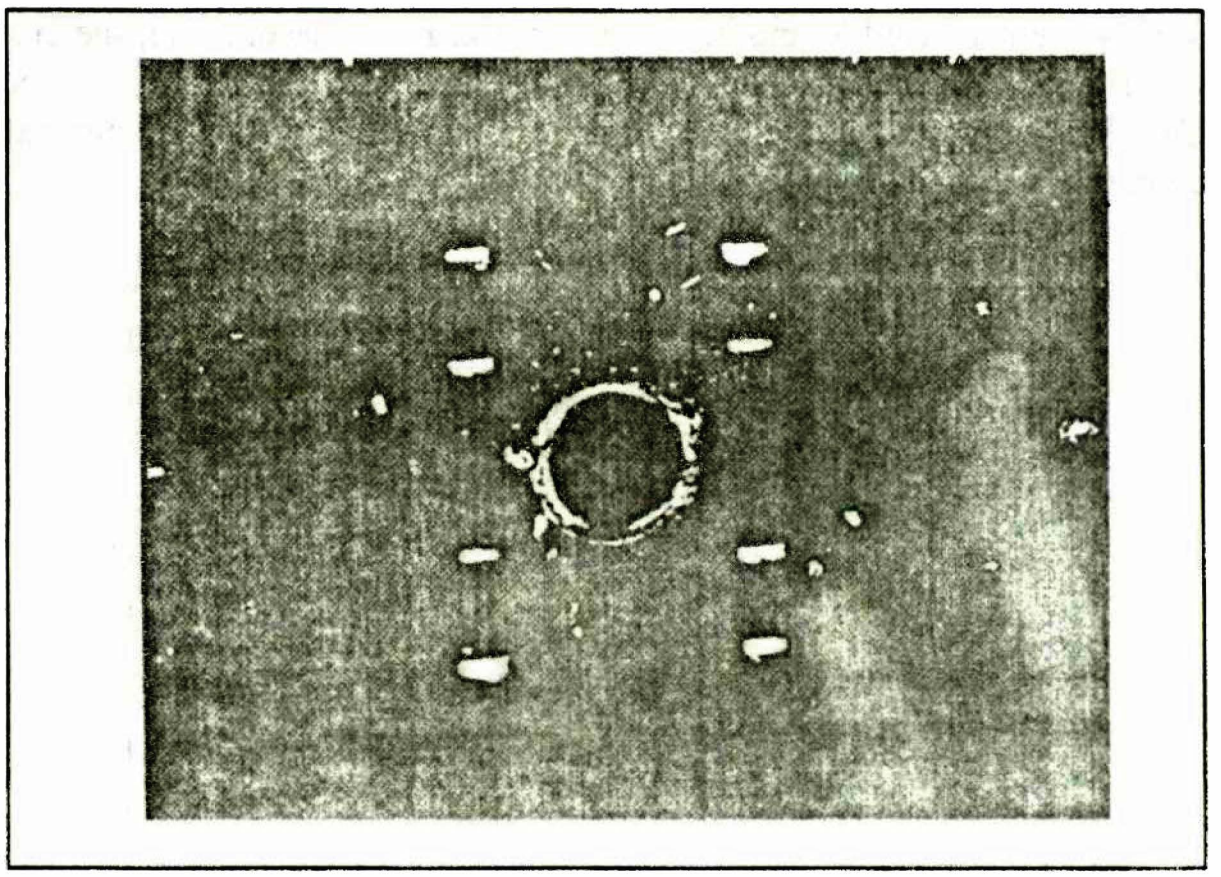

Figure 4. Laue diffraction pattern of the well-developed (110) plane of $ZnSe_{0.92}S_{0.08}$

X-ray Diffraction by $ZnSe_xS_{1-x}$ Single Crystals

Experimental Procedure and Results

For an x-ray spectrometer based upon Bragg's analysis, a collimated beam of x-rays falls upon a crystal at an angle θ, and a detector is placed so that it records those rays whose scattering angle is also θ. Any x-rays reaching the detector therefore obey the first Bragg condition. As θ is varied, the detector will record intensity peaks corresponding to the orders predicted by Bragg's law. Since the x-ray wavelength λ is known; the spacing d between adjacent Bragg planes in the crystal can be calculated.

The grown crystals are cut and ground and the crystallites are set in a flat lead base. The prepared sample is mounted on the x-ray apparatus using Cu as a target. The x-ray spectrum is fully recorded on a chart.

Figure 5 shows the x-ray diffraction spectra of ZnSe, $ZnSe_{0.92}S_{0.08}$, $ZnSe_{0.83}S_{0.17}$, and $ZnSe_{0.50}S_{0.50}$. The said spectra show the well-defined zincblende

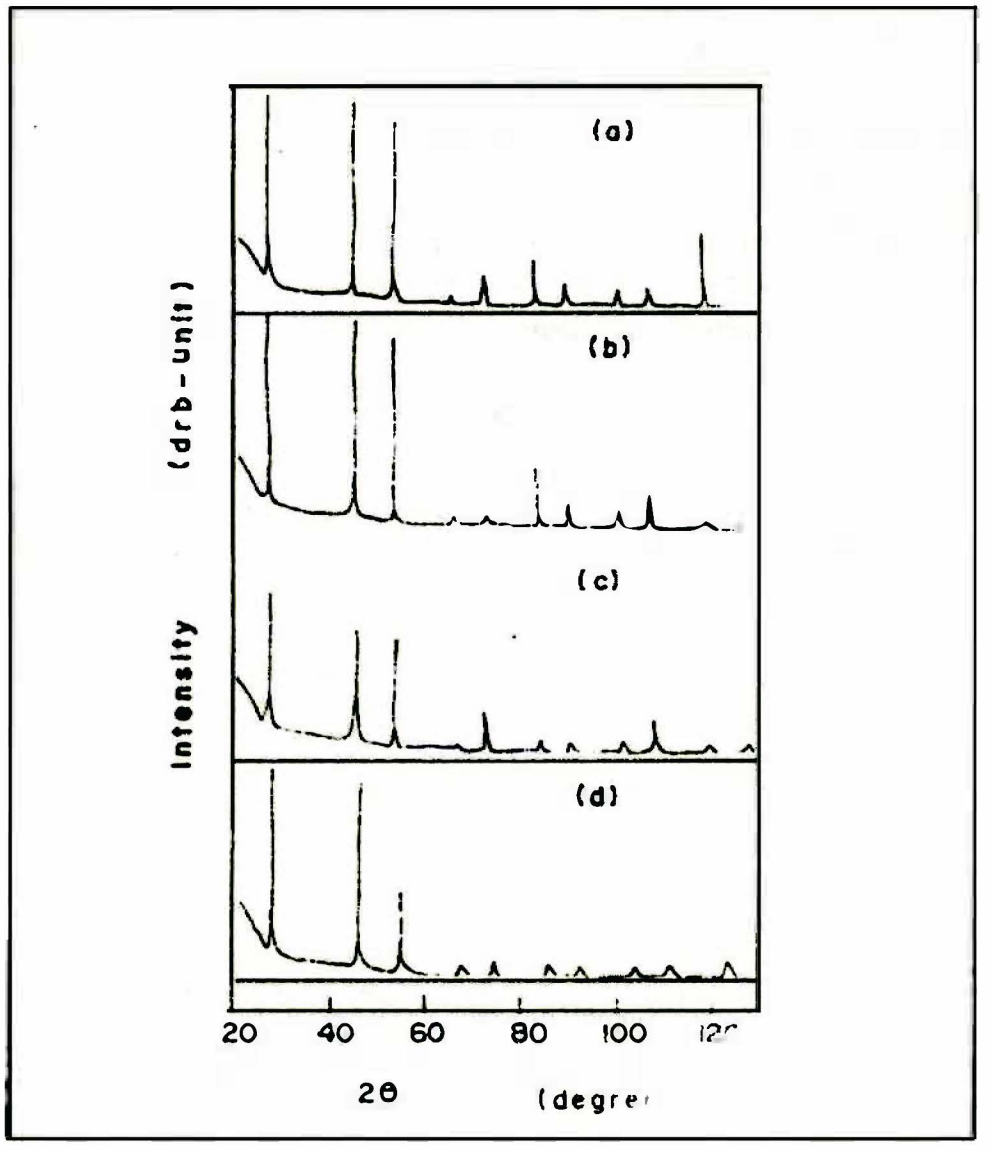

Figure 5. X-ray diffraction spectra of (a) ZnSe, (b) $ZnSe_{0.92}S_{0.08}$, (c)$ZnSe_{0.83}S_{0.17}$, (d) $ZnSe_{0.50}S_{0.50}$.

structure of $ZnSe_xS_{1-x}$ single crystals. The lattice constants of $ZnSe_xS_{1-x}$ single crystals obtained from x-ray diffraction spectra as related to the ZnSe composition of the crystals are shown in Fig. 6. The lattice constants are calculated using Bragg's law[36]. It is confirmed that the lattice constant varies linearly with the increase of ZnSe component. These results affirm that Vegard's law holds for our ternary compound with the zincblende structure. The minimal deviation from the relationship can be explained by experimental bias in measuring the diffraction angle in the x-ray apparatus. Furthermore, the crystals are grown by the self-closed sublimation method where the growth tube is open at the start of growth. It is very plausible that the composition of the homogeneous ternary compound may have been altered at this stage of growth.

III. PHOTOLUMINESCENCE SPECTRA OF ZnSexS1-x

ZnSe and ZnS are II-VI compounds which have the zincblende structure at room temperature. The lattice constant of ZnSe is 5.6676 Å while that of ZnS is 5.4093 Å. at 300K, the energy gap of ZnSe is 2.67 eV and that of ZnS is 3.76 eV. ZnSe and have n-type conduction and it is very difficult to convert the conduction type due to the self-compensation effects which are caused by native defects produced as a consequence of dopant atom incorporation[1] and the presence of residual impurities, which make it difficult to control the conductivity.

The near bandgap emission of ZnSe and ZnS consists of three different groups of bands at low temperatures. One of these groups is due to the radiative annihilation of free excitons and their corresponding LO-phonon replicas. The

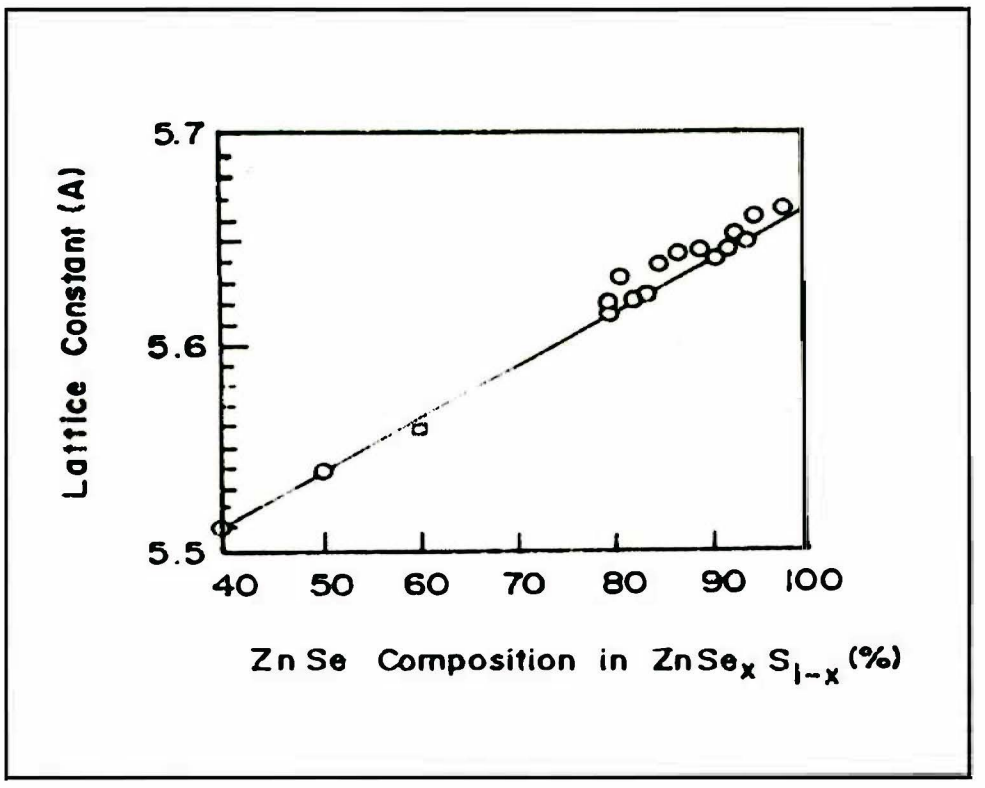

Figure 6. Lattice constant vs. ZnSe composition in $ZnSe_xS_{1-x}$.

second group is attributed to emission from bound exciton complexes and their associated phonon replicas. Finally; the third group consist of a relatively broad band emission occurring at somewhat lower energies.

An action emission causes the sharp-line spectrum near the band edge. This emission is only observed at low temperatures. An exciton is an electron-hole pair bound together by their attractive electrostatic interaction. The electron and hole orbit around their common center of mass in quasi-hydrogen orbitals. The exciton can move through the crystals transporting excitation energy, but it is electrically neutral. They can formed in every insulating crystal, although some types of excitons are intrinsically unstable with respect to decay into a free electron and a free hole. All excitons are unstable against the ultimate recombination process in which the electron drops into the hole.

The exciton is not spatially localized since it is free. The energy E_{ex} of an exciton is generally represented relative to the conduction in bandedge, E_{ex} ($N = \infty$) being the conduction band energy. When the free exciton recombines, the emitted energy is

$$h\nu = E_g - E_{ex}^{free} \tag{1}$$

where Eg is the band gap energy and E_{ex}^{free} is the ionization energy for the free exciton, relative to the conduction and valence band electron and hole states which are analogous to the free electron states in the hydrogen atom model. The translational kinetic energy of the free exciton which broadens the observed transition is neglected in this expression.

Bound excitons occur in materials which contain defects or impurities. A free exciton may be trapped at the impurity or defect or a free hole may combine with a neutral donor to form a positively charged ion[1]. In this case, the electron travels about the donor atom in a wide orbit, and the hole moves in the dipole field of the orbiting electron. The luminescence due to the recombination of an electron-hole pair captured by a neutral acceptor is called an I_2 line. That of an electron-hole pair captured by an ionized donor is called an I_3 line. The trapped electrons possess modified orbitals which are characteristic of the trapping center. Consequently, the trapped exciton provides additional information about the center when it decays. The emitted energy for the bound exciton is

$$h\nu = Eg - E_{ex}^{free} - E_{ex}^{b} \tag{2}$$

where E_{ex}^{b} is the energy binding the exciton to the defect center.

An exciton can be captured by the ground state of an ionized donor-acceptor pair. The luminescence as this exciton recombines is called the donor-accepter luminescence which is one of the dominant radiative recombination mechanism at low temperature for II-VI semiconductors. The schematic models of excitons are shown in Fig. 7.

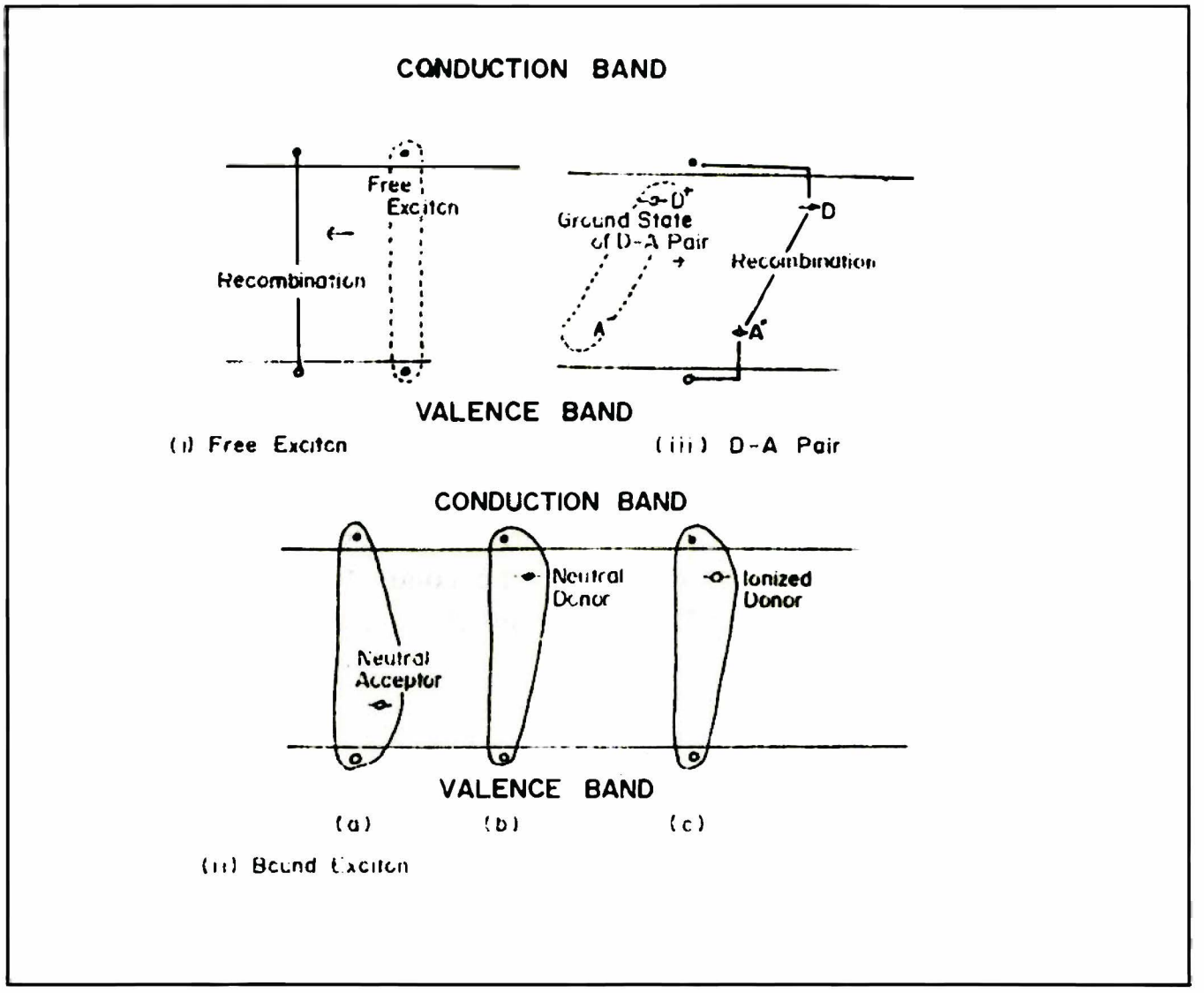

Figure 7. Schematic models of excitons (i) free exciton, (ii) bound exciton captured by (a) a neutral acceptor, (b) a neutral donor, and (c) an ionized donor (iii) free exciton captured by the ground state of a donor-acceptor pair.

Measurement of Photoluminescence Spectra of $ZnSe_xS_{1-x}$

The samples used in this study are formed to about 5x4x2 mm^3 by cleaving and cutting from as-grown crystals. Half of these as-grown crystals are directly used in the measurement and the rest undergo further heat treatment.

Several of the prepared crystals of different compositions are prepared by firing in molten zinc for 24 hr at about 900°C in an evacuated quartz crucible. Prior to the heat treatment, the cleaved and cut crystals are polished with a solution of TiO_2 and are purified by an ultrasonic cleaner to remove excess powder. After firing in molten zinc, the crystals are quenched to anneal. Previous to the optical measurements, the samples are etched in a 30% NaOH solution boiled to remove the zinc which adhered on the surface of the crystals after the heat treatment.

The luminescence spectra are measured at 4.2 K with the crystals immersed directly in liquid helium in a glass cryostat which itself is immersed in liquid nitrogen.

The photoluminescence spectra of the $ZnSe_xS_{1-x}$ single crystals are measured using the holographic concave grating monochromator (HR-1000 produced by Yvon Jobin Optical Systems) with the 1200-groove/mm grating which has a dispersion of 0.8 nm/mm. A photomultiplier (R562 produced by Hamamatsu Photonics Co., Ltd.) is used as a detector. The luminescence is excited by uv-light from either a 365-Hg lamp or a 1.0kW Xe lamp through a Toshiba UV-D1B filter and cupric sulfate aqua. The schematic diagram of the experimental set-up for the measurement of the photoluminescence spectra of the ZnSexS$_1$-x single crystals is shown in Fig. 8.

Results

Figure 9 (a) shows the photoluminescence spectrum of as-grown $ZnSe_{0.96}S_{0.04}$ I_2 and I_1^{deep} accompanied by LO phonon replicas are very prominent and no DAP band is present. However, as shown in Fig. 9 (b), the same crystal annealed in Zn vapor, the intensity of the I_1^{deep} line diminishes appreciatively with respect to the I_2 line. The I_1^{deep} line is known to be due to the recombination of excitons bound to neutral acceptors. The aforementioned acceptors are considered as Zn vacancies (V_{zn}) or associated defects containing V_{zn} (V_{zn}- complex)[9]. The decrease in the

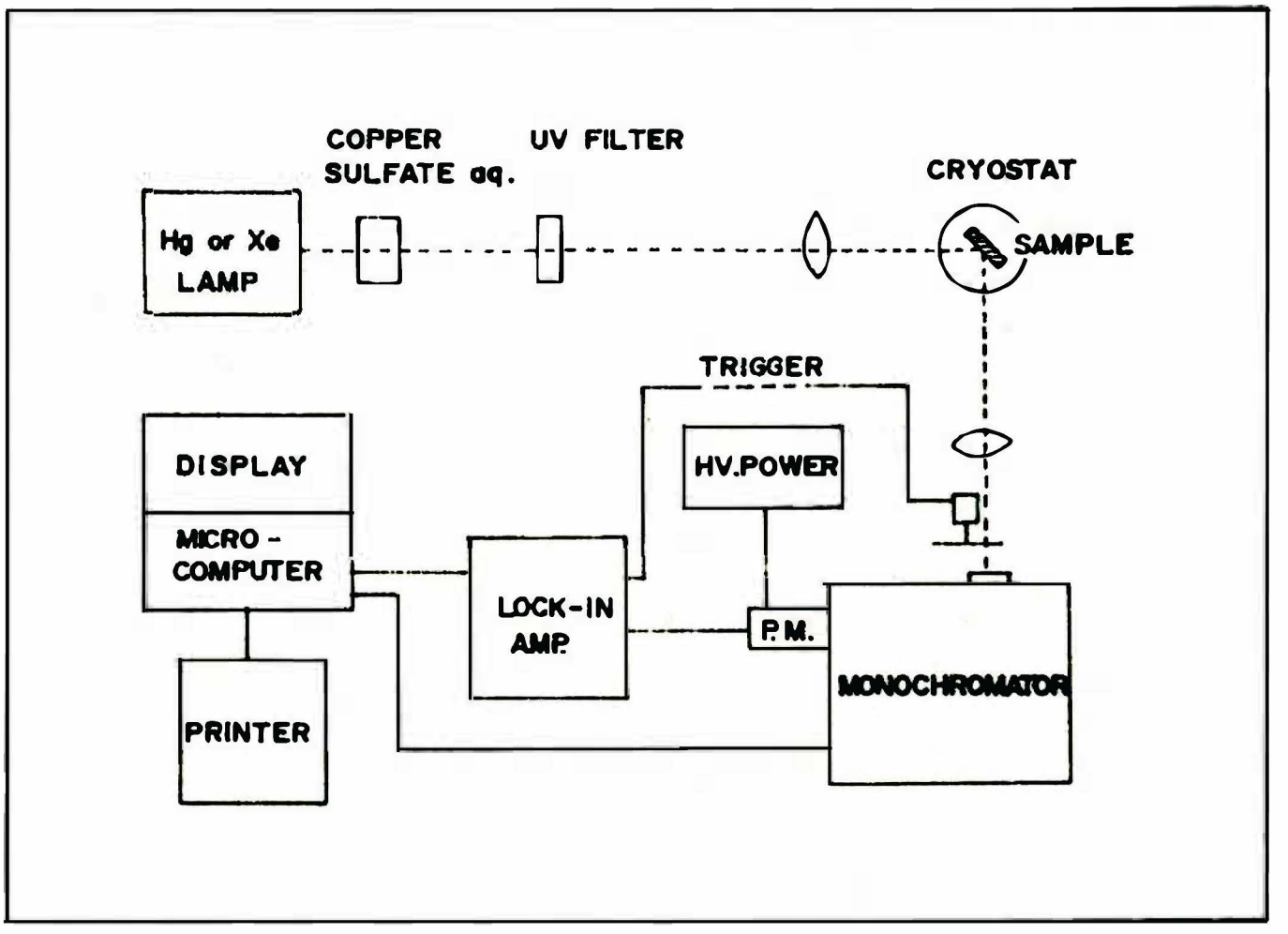

Figure 8. Schematic diagram of the measurement system used to observe the photoluminescence spectra.

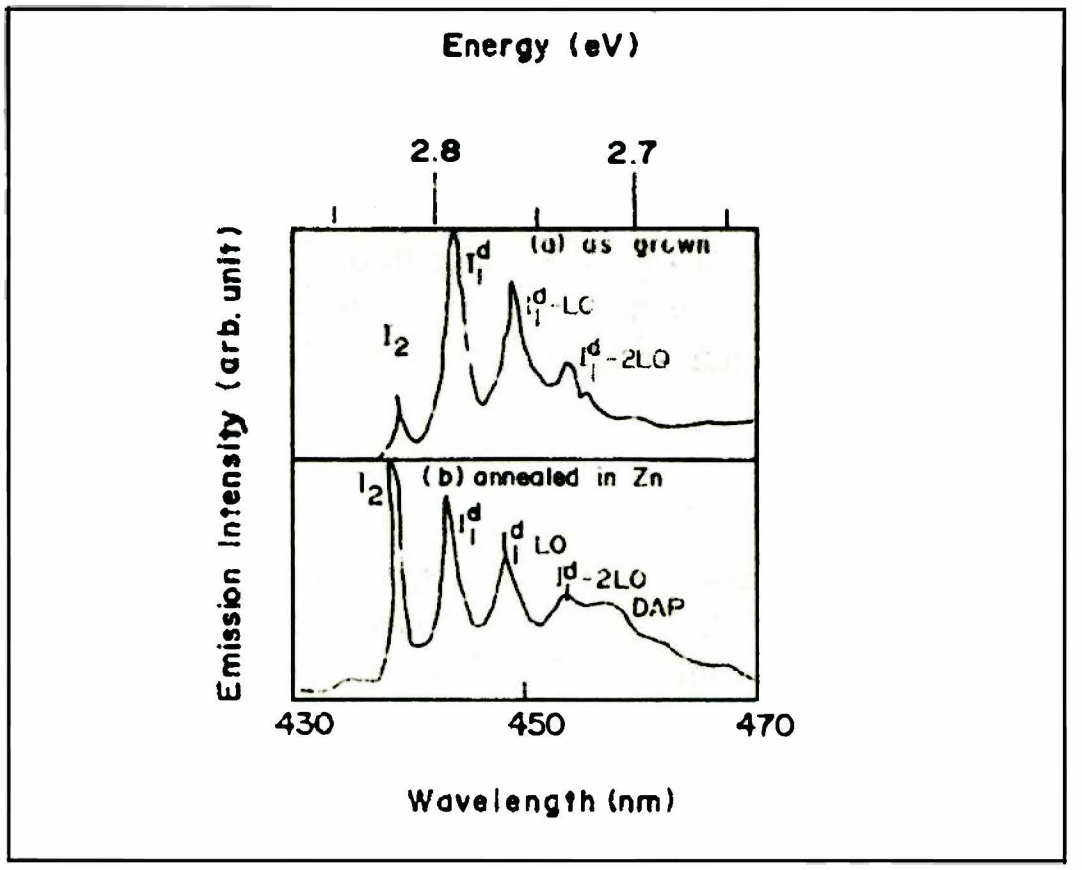

Figure 9. Photoluminescence spectra of $ZnSe_{0.96}S_{0.04}$

intensity of the I_1^{deep} line therefore can be explained by the decrease in the density of the Zn vacancies after heat treatment in Zn vapor. The DAP pair luminescence band is also observed. The difference between the I_1^{deep}-LO phonon replicas is approximately 31.5 ± 1 meV which can be assigned as the value of the LO phonon energy for $ZnSe_{0.96}S_{0.04}$.

The photoluminescence spectra of Li-doped $ZnSe_xS_{1-x}$ ($0.81 \leq x \leq 1$) samples are shown in Fig. 10. For the x = 1 sample, the observed band at 2.696 eV (Q_o) is attributed to the presence of Li, confirming earlier conclusions of Merz et al.[37]. A weak bound exciton line is also present with the 2.696 eV band. The peak is ascribed to be I_1^{deep} which is the luminescence due to the recombination of an electron-hole pair captured by a neutral acceptor which is assumed to be either a Zn vacancy or a V_{zn}-complex. It is very evident in the figure that the emission energy shifts to the lower energy side as the ZnSe composition x in the $ZnSe_xSe_{1-x}$ increases. For the x = 0.81 sample the bound exciton line becomes more prominent with an emission energy of 2.914 eV. A free exciton line is also observed at 2.946 eV. The Q_o-DAP band for x = 0.86 is 2.765 eV.

The effects of Na- as well as Li-doping are evaluated. As shown in Fig. 11, no DAP band is present in the as-grown sample. A P_o-DAP however, is observed in the Na-doped sample at 2.795 eV. For the same ZnSe composition of 0.81, a DAP band of different emission energy of 2.807 eV is observed for the Li-doped sample. This band is assigned as Q_o which is due to the transition involving Al_{zn^+} donor and Li_{zn^-} acceptor which agrees with Merz et al.[37]. The presence of the Al donor is determined by secondary ion microanalysis spectroscopy (SIMS) as shown

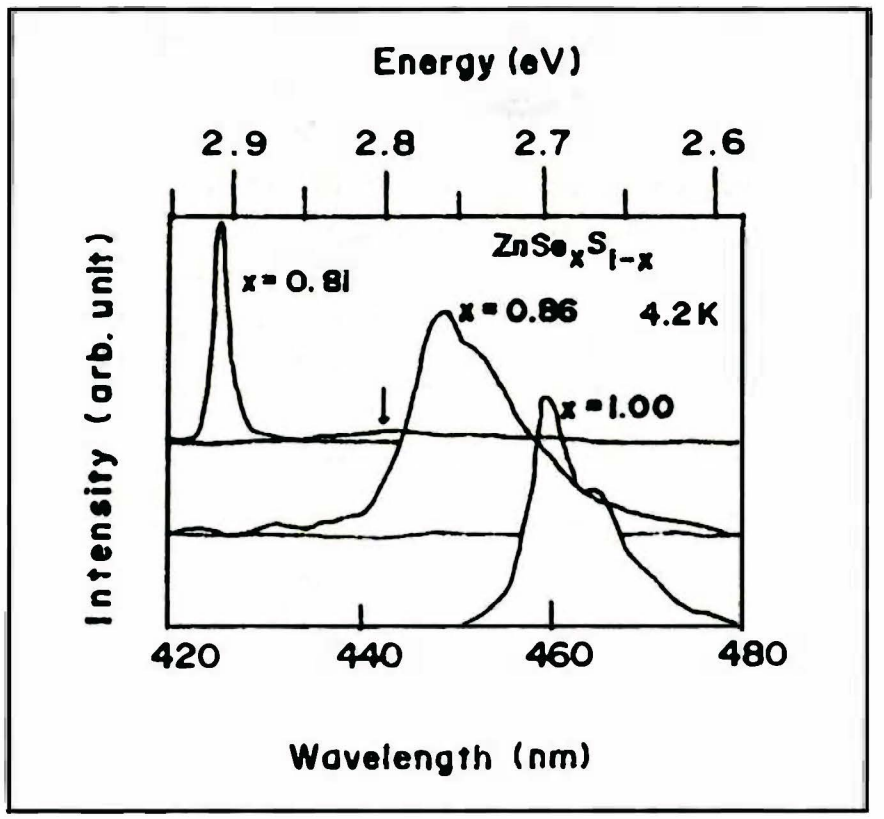

Figure 10. Photoluminescence spectra of Li-doped $ZnSe_xS_{1-x}$

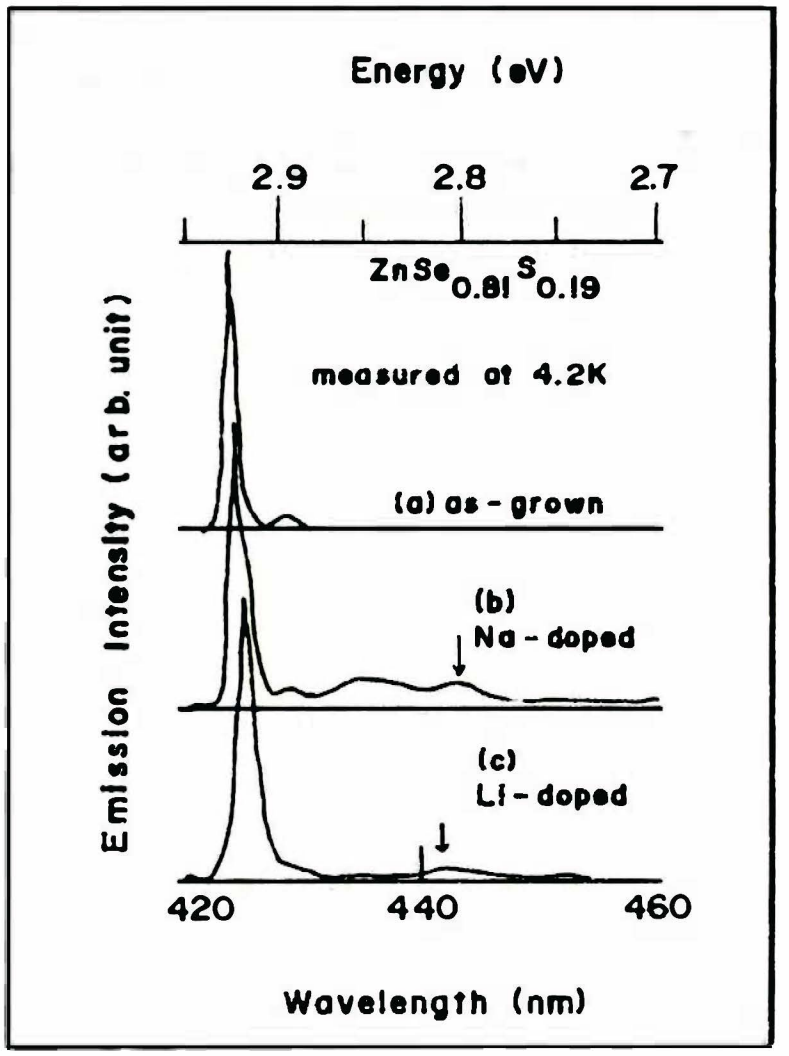

Figure 11. Photoluminescence spectra of $ZnSe_{0.81}S_{0.19}$ (a) as grown, (b) Na-doped; (c) Li-doped.

in Fig. 12. The Q_0-DAP band occurs at 13 meV higher energy than the P_0-DAP band which may be explained by the difference in the acceptor binding energies of Na and Li with Al as the common donor in both samples. I_1^{deep} is strong in all samples which is an indication that the concentration of neutral acceptors is high. E_x which is due to the radiative annihilation of free excitons is barely discernable in the Li-doped sample and its presence is not detected in the other samples. Since all samples have high concentrations of V_{zn} (acceptors in the high-intensity I_1^{deep}), the excitons bind to the V_{zn} or V_{zn}-complex.

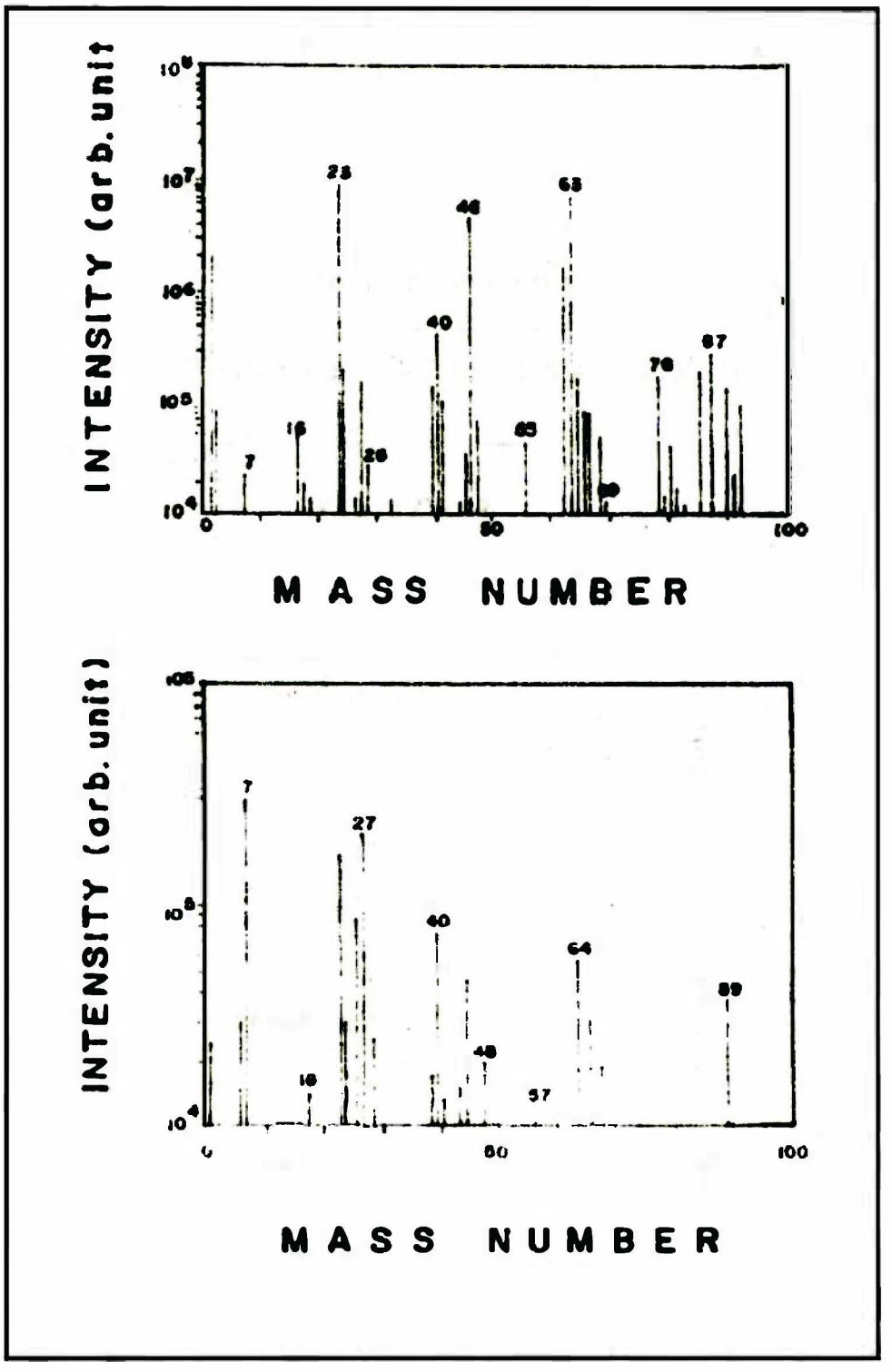

Figure 12. SIMS results for (a) Na-doped $ZnSe_{0.81}S_{0.19}$ and (b) Li- doped $ZnSe_{0.81}S_{0.19}$

The photoluminescence spectra of the as-grown $ZnSe_xS_{1-x}$ ($0.80 \leq x$ 7 0.96) is shown in Fig. 13. As the ZnSe composition increases, the respective energies of the emission peaks of I_2 and I_1^{deep}, the DAP band and its corresponding LO-phonon replicas shift to the lower energy side. E_x is not observed in the figure. However, bound exciton lines are remarkably present. For $x = 0.93$, the relative intensities of the peaks of the donor- as well as the acceptor-bound excitons are very strong with the emission of the acceptor-bound exciton accompanied by the LO-phonon processes which result due to strong coupling to the lattice. The LO-phonon energy in this sample is 30.0 ± 1 meV. For 0.91, I_2, I_1^{deep}, and DAP band are observed. The broadening of the bands is due to the merger of the LO-phonon replicas of both I_1^{deep} and the DAP band. The broadening of the I_1^{deep} in the samples $x = 0.96$, 0.93, and 0.86 can be explained by the increase of irregularity due to the inclusion of sulfur (S) in ZnSe.

The relationship between the respective emission energies and the ZnSe composition in $ZnSe_xS_{1-x}$ is shown in Fig. 14. It is clearly seen that the corresponding emission energies decrease curvilinearly with the increasing ZnSe composition x. Strong DAP emission observed for $0.91 \leq x \pm 0.96$ can be explained by the fact that a different preparation procedure for the starting material is adopted; i.e., KCl is used as flux.

Shift Of Luminescence Peak With Excitation Intensity

To identify the series of broad bands in the low energy side of the luminescence spectra of the as-grown samples annealed in Zn vapor as well as the

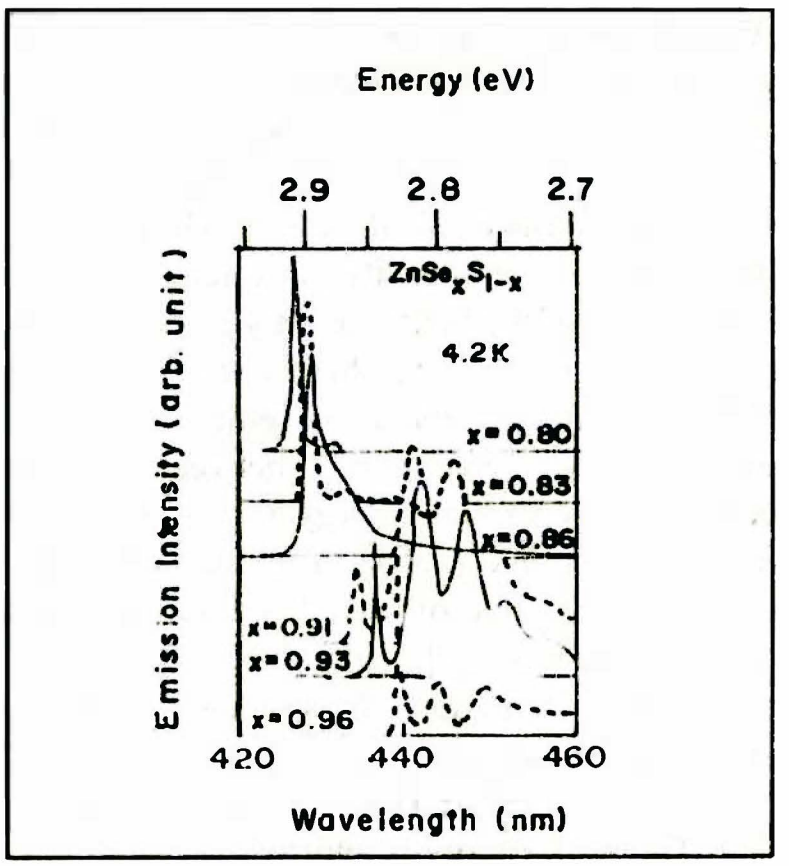

Figure 13. Photoluminescence spectra of $ZnSe_xS_{1-x}$ ($0.80 \leq x \leq 0.96$)

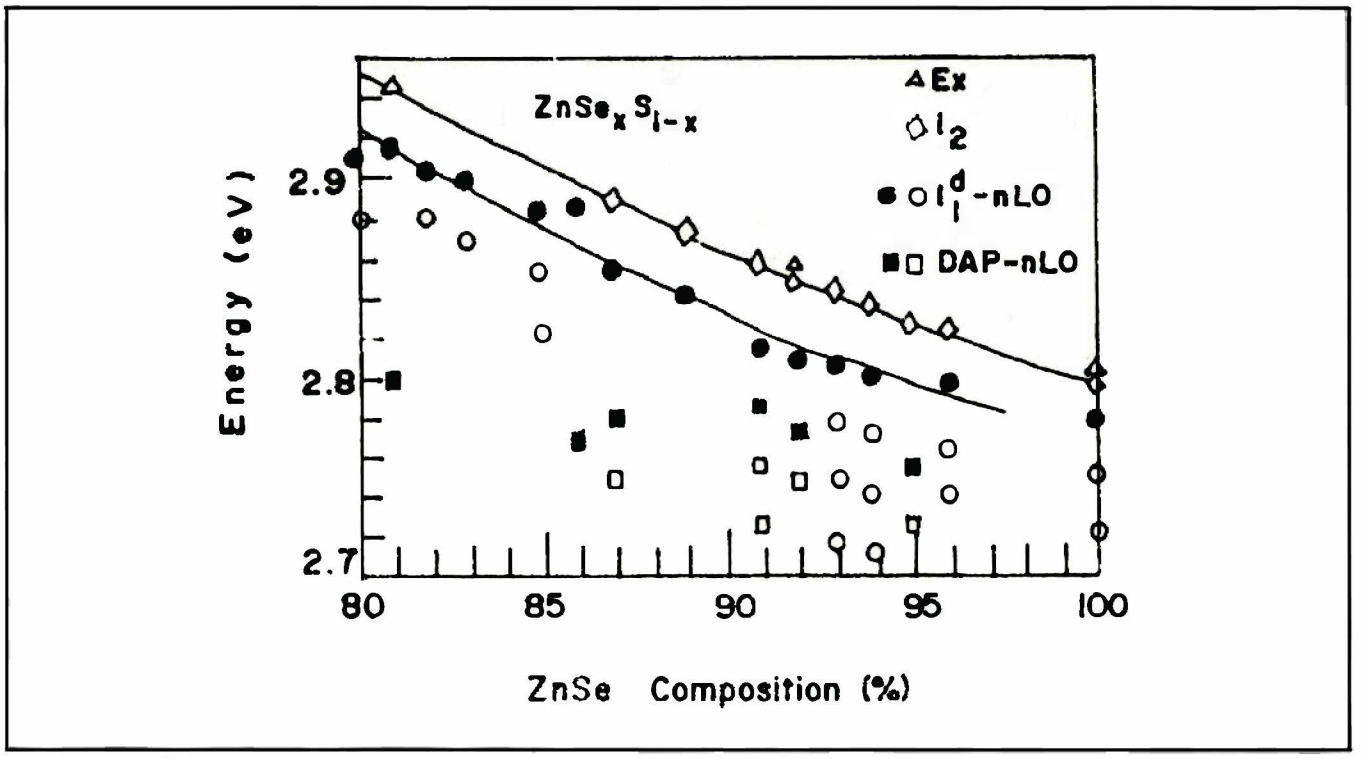

Figure 14. ZnSe composition dependence of emission energies

purposedly Na- and Li-doped samples, excitation measurements are undertaken. The luminescence is excited by a 1kW Xe lamp with a uv filter. The schematic diagram of the experimental set-up is previously shown in Fig. 8.

It is consistently observed as in Fig 15(A) for an as-grown $ZnSe_{0.92}S_{0.08}$ crystal that the donor-acceptor pair band and its accompanying LO phonons shift to higher energies with increasing excitation. In Fig. 15(B), the aforementioned behavior is also observed in addition to the fact that the bands broaden as the excitation intensity is increased at a fixed temperature of 4.2 K.

It is assumed that the broad band in the as-grown $ZnSe_{0.92}S_{0.08}$ sample is due to the recombination of remote donor-acceptor pairs where the donor is Al and the acceptor is Na on the basis of SIMS results. The peak of this band shifts to higher energies with increase in the intensity of excitation.

In Fig. 15(B), the peak of the band not only shifts to higher energies as the excitation intensity increases but also the high-energy tail of the band broadens due to saturation of the transitions at relatively remote pairs where the pair transition energy hv depends on the separation R between the donor, of ionization energy E_D, and acceptor, of ionization energy E_A in agreement with Thomas et al.[54]. The acceptor involved in the transition in Fig. 15(B) is believed to be Li since the band has the characteristic of a Q_0 band assigned to a Li-acceptor and further confirmed by SIMS results. Although the peak energy of this band shifts to higher energy with increasing excitation intensity, the rate of increase is at slightly less than half of that of the P_0 band with Na as the acceptor as in Fig. 15(B).

Figure 16 shows the shift of the D-A pair-LO phonon band with the intensity of Xe excitation. The peak energy is approximately related to a power of the excitation intensity such that a shift of ~ 4.7 meV for the as-grown $ZnSe_{0.92}S_{0.08}$

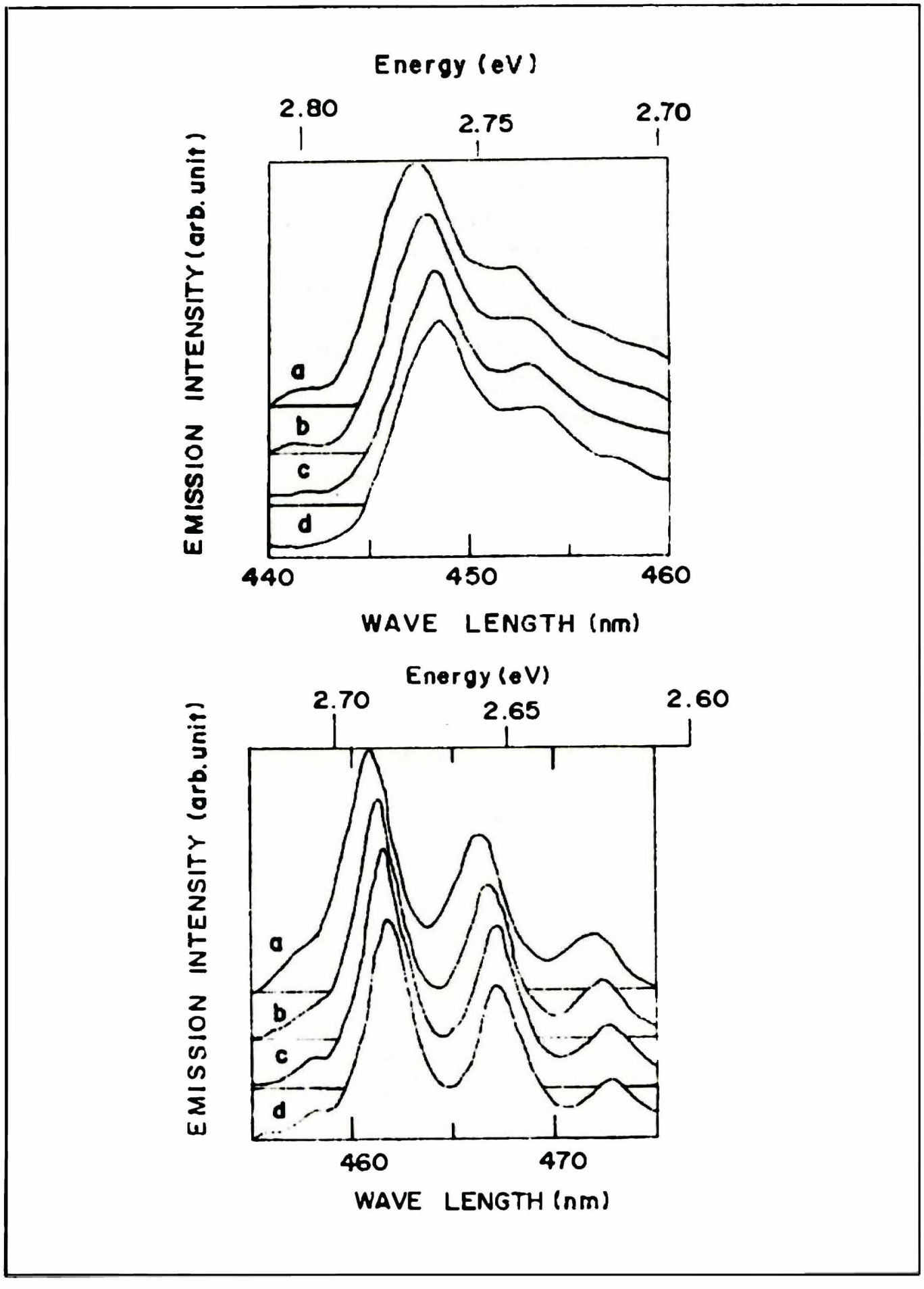

Figure 15. Photoluminescence spectra of (A) $ZnSe_{0.92}S_{0.08}$ and (B) Li-doped ZnSe excited by 1 kW Xe lamp (a) initial intensity I_0 (b) $I_0/4$ (c) $I_0/16$ and (d) $I_0/32$.

sample annealed in Zn vapor (Fig. 16(a)) and ~ 2.9 meV for the Li-doped sample are respectively caused by a tenfold increase in intensity. These are of the order of the shift observed in the peak intensity of their pair spectra in CdS[49] where the shifting has been attributed to saturation of distant donor-acceptor pairs states with long lifetimes and is considered a donor-acceptor recombination.

In order to analyze the energies of the pair transition using the hydrogenic model, it is necessary to assign values of the pair separation to the observed peaks. It is done by assuming that the relative intensities of neighboring peaks are proportional to the statistical probability that a particular pair should occur, assuming a random distribution of impurities. The intensity patterns for a zincblende lattice as calculated by Hopfield[38] are used in which both the donor and acceptor occur on the same type of substitutional or interstitial site in either the zinc or selenium sublattices.

The binding energy of the Li acceptor is estimated from the rule of Halsted and Aven[55] and is found to be 110)5 meV where the donor-acceptor pair band due to a Li acceptor has an emission energy which is about 13 meV higher than that of a donor-acceptor pair due to a Na acceptor.

IV. EXCITATION SPECTRA OF A DONOR-ACCEPTOR PAIR

The excitation processes by light illumination to generate the excited donor-acceptor pair states are classified into three categories, viz.:

(i) band-to-band transition,
(ii) transition from the acceptor to the conduction band (bound-to-free transition) and

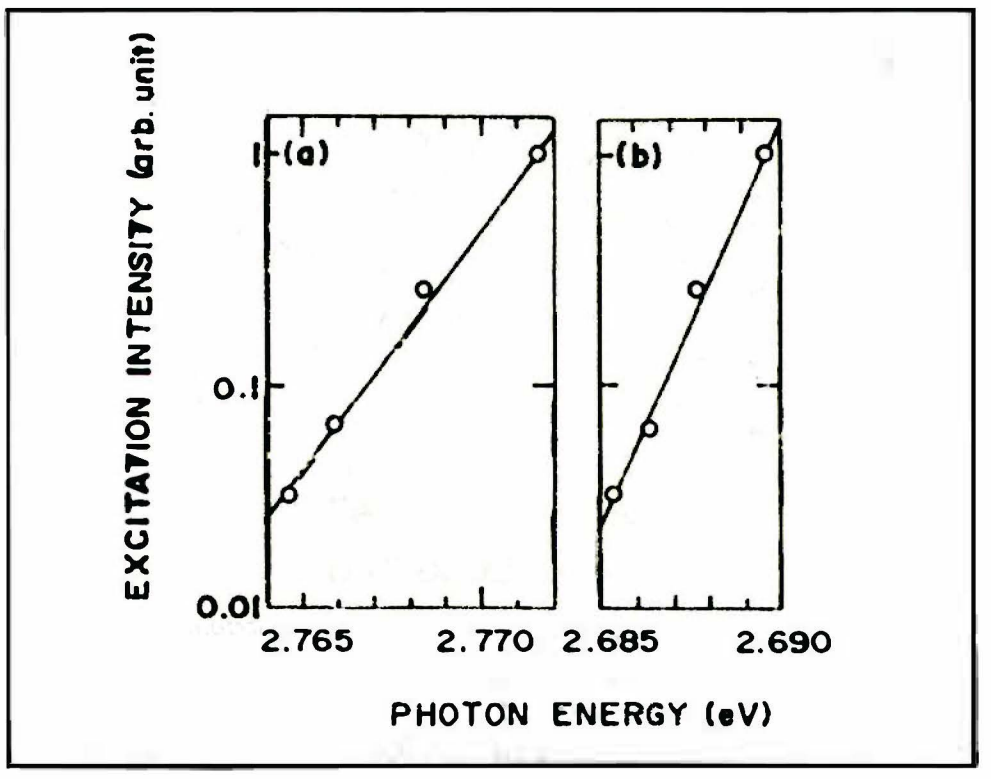

Figure 16. Excitation intensity dependence of the (a) Po peak position in as-grown $ZnSe_{0.92}S_{0.08}$ and the (b) Qo peak position in Li-doped ZnSe.

(iii) transition within donor-acceptor pair.

The models for donor-acceptor pair luminescence are shown in Fig. 17. The third process is observed under the condition of below bandgap excitation.

Band-to band Transition

Free electrons and holes are created by photons with energies greater than the bandgap energy E_g. The free carriers are first captured by ionized centers with the larger capture cross section. At very low excitation intensities, the recombination is not limited by the radiative recombination probability, but by the capture cross section. Hence, the emission intensity is determined by the capture cross section and the pair distribution function.

Bound-to-free Transition

For the donor-acceptor pair with distance R, an electron is excited into the conduction band leaving a hole in the acceptor ground or excited states when R satisfies the following condition for a given photon energy hv

$$E_g - E_A + \frac{e^2}{\varepsilon R} \leq h\nu \qquad (3)$$

where E_g is the bandgap energy, E_A the binding energy of the acceptor, and ε the static dielectric constant. For this process, the donor-acceptor pairs which satisfy

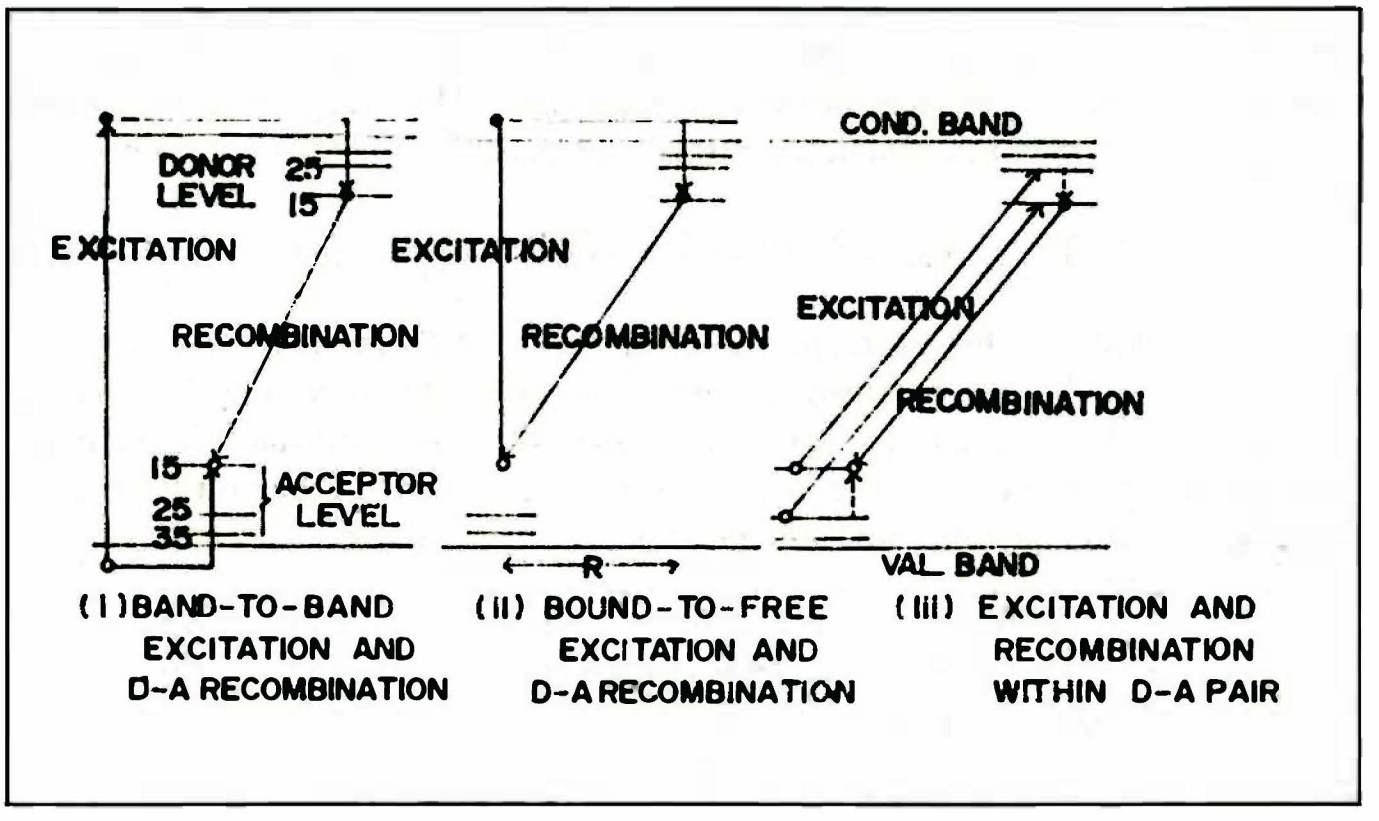

Figure 17. Excitation processes by light illumination to generate the excited donor-acceptor pair states

the above condition are positively charged and the free electron captured immediately.

Transition within D-A Pairs

The photon energy necessary for this excitation of the donor-acceptor pair with sufficiently distant pair separation R at very low temperature is given by

$$h\nu(R) = E_g - \left(E_n^D + E_m^A\right) + \frac{e^2}{\varepsilon R} + \Sigma\, nh\nu_i \tag{4}$$

where E_n^D and E_m^A are the binding energies of the donor and the acceptor in respective quantum states n and m; and $h\nu_i$ is the energy of the i-th phonon emitted in transition.

If it is assumed that the recombination occurs between electrons bound to the 1s state and holes bound to the acceptor 1s state, the emitted photon energy is given by

$$h\nu_e(R) = E_g - \left(E_1^D + E_1^D\right) + \frac{e^2}{\varepsilon R} - \sum_{p,j} nh\nu_j \tag{5}$$

where $h\nu_j$ is the phonon energy emitted at the recombination. The electrons and hole at the exciled states are relaxed radiatively or non-radiatively to the grounds states of each impurity level.

The photon energy necessary for the excitation of a donor-acceptor pair and the emitted photon energy are given in equations (4) and (5). Distribution of the donor-acceptor pairs with various separations give rise to a broad band.

For the excitation process, it is possible to excite an electron to the donor excited state leaving a hole in the acceptor ground state or to the donor ground state leaving a hole in the acceptor excited state. The difference between equations (4) and (5) gives the excited state energies of the acceptor and the donor, i.e.

$$h\nu(R) - h\nu_e(R) = \left(E_1^D - E_n^D\right) + \left(E_1^D - E_m^A\right) + nh\nu_i + nh\nu_j \tag{6}$$

It is noteworthy that this expression is independent of R. Furthermore, this relation includes neither the bandgap nor the coulomb energy, therefore this enables us to analyze the excited state of shallow impurities in a crystal of which the bandgap energy and dielectric constant are not well known. Equation (6) can be expressed in two equations since the electron transition occurs in a donor atom or an acceptor one. That is

$$h\nu(R) - h\nu_e(R) = E_1^D - E_n^D + nh\nu_i \tag{7}$$

$$h\nu(R) - h\nu_e(R) = E_1^A - E_n^A + nh\nu_j \tag{8}$$

From the difference between the observed wavelength and the excited wavelength, the energy difference of atomic energy states of a donor or acceptor is obtained.

Phonos

The energy of a lattice vibration is quantized. The quantum of energy is a called a phonon in analogy with the photon of an electromagnetic wave. Thermal vibrations in crystals are thermally excited phonons, like the thermally excited photons of blackbody electromagnetic radiations in a cavity.

Elastic or acoustic phonons are thermal vibrations with low frequencies which can occur only when neighboring lattice components move approximately in phase. Optical phonons are thermal vibrations which occur when neighbors have opposite electric charge leading to a high frequency electric dipole moment and consequently the emission of an electromagnetic wave.

A general feature of both exciton and pair emission spectra in II-VI compounds is that almost all emissions appear as a series of lines separated by equal energy increments which is caused by strong coupling to the lattice which results in more radiative processes being accompanied by phonon emission processes. In most of the II-VI compounds, the most probable phonon to be emitted is the longitudinal optical (LO) phonon. For strong emission lines, one finds a transition corresponding to the emission of n=1, 2, 3,... phonons. The phonon coupling and the broadening by a high concentration of donor-acceptor states explain the observed broad band transitions.

Hopfield[38] has shown that the intensities of the phonon replicas generally can be described by the relation

$$I_n = I_o \left(\frac{\bar{N}^n}{n!} \right) \tag{9}$$

where I_n is the relative intensity of the n+1 lines of the set involving the emission of a photon plus n-LO phonons. $\bar{N}$, the mean number of emitted LO phonons given experimentally by the ratio $I_1 = I_o$, provides a measure of the coupling of the center to the lattice.

Experimental Procedure and Results

It is significant to know the energies of donors and acceptors to understand the optical properties of $ZnSe_xS_{1-x}$. The centers in $ZnSe_xS_{1-x}$ ($0.85 \leq x \leq 1$) by excitation spectroscopy on D-A pair bands are discussed.

The excitation spectra of D-A pairs are measured by a dye laser pumped with the third harmonics of a Q-switched Nd^{3+}:YAG laser. The output signals from a photomultiplier are accumulated by a boxcar integrator. During measurements, the crystals are immersed in liquid helium bath. The schematic diagram of the excitation spectra of $ZnSe_xS_{1-x}$ using Nd^{3+}:YAG laser is shown in Fig. 18

Examples of excitation spectra for a D-A pair band in $ZnSe_xS_{1-x}$ (x=0.94) are shown in Fig. 19. The observed wavelengths of the D-A pairs are indicated by arrows.

Excitation and recombination processes of donor-acceptor pairs in the present excitation spectra are shown schematically in Fig. 20. One donor-acceptor pair separated by R_{DA} is considered and the excitation processes are as follows: Excitation of the acceptor electron in its ground state E_A to the donor ground state E_D accompanied by the emission of one TO or LO phonon [process (b) or (c)], or two LO phonons [process (d)]. Excitation of the acceptor electron in its ground state E_A into the excited state of the donor E_D^*, and then the donor electron relaxes to its ground estate E_D [process (a)]. Excitation of the acceptor electron in its excited E_A^* to the ground state of the donor, then the hole left in the excited state of the acceptor relaxes to its ground state [process (e)]. Recombination takes place between the donor electrons and the acceptor hole each in its ground state, emitting luminescence.

In Fig. 21, energy differences between observed D-A pair and the peak energies appearing in the excitation spectra are plotted as a function of the observed wavelength of the D-A pairs. Although the D-A pair luminescence from different pair separations are observed, the dip is always observed at 436.5 nm in the spectra (cf. Fig. 19), and this is due to the absorption creating free excitons. This dip also corresponds well to the dip appearing in the reflection spectrum. Fig. 21 indicates that all peaks relative to the observed D-A pair have correspondingly constant energy separations, which means eq. (11) holds. The lowest energy peak

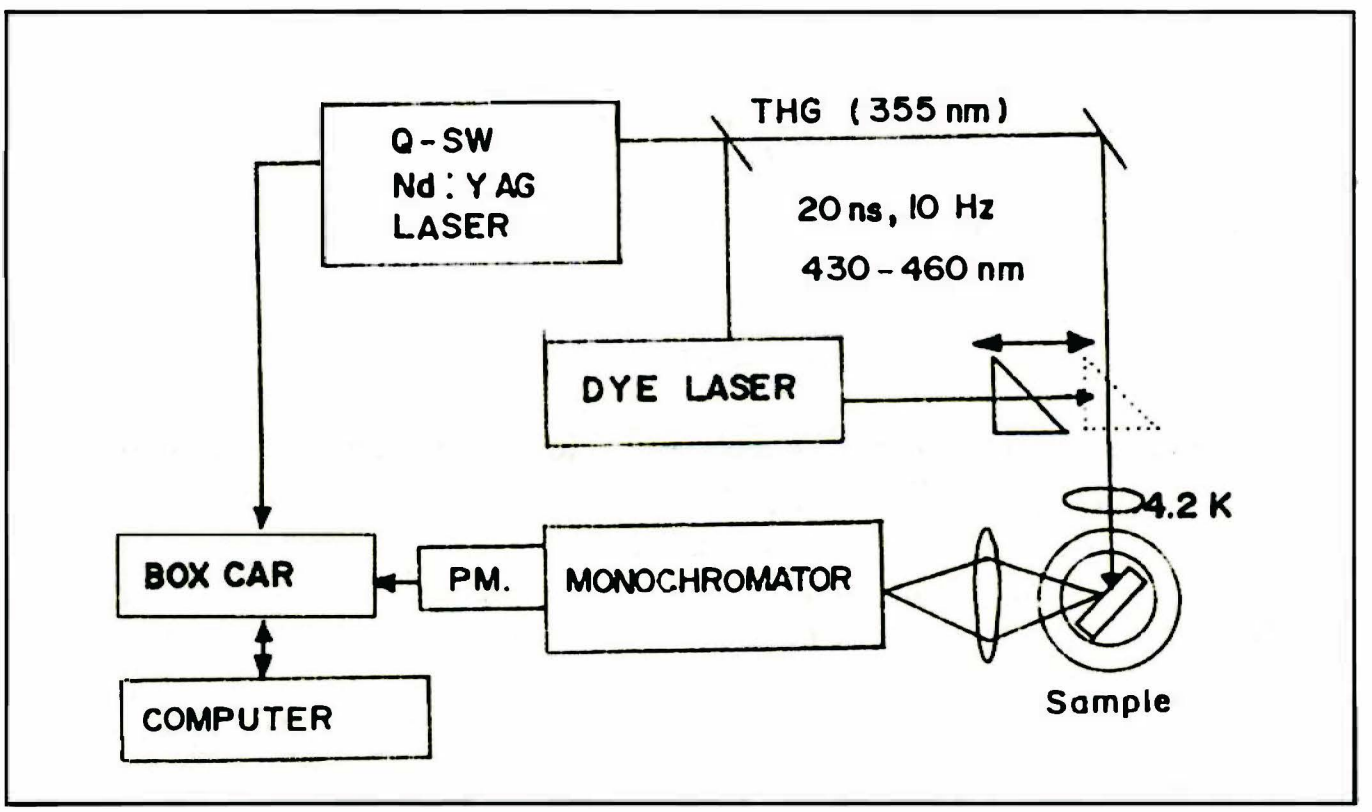

Figure 18. Schematic diagram of the measurement system used to observe the excitation spectra.

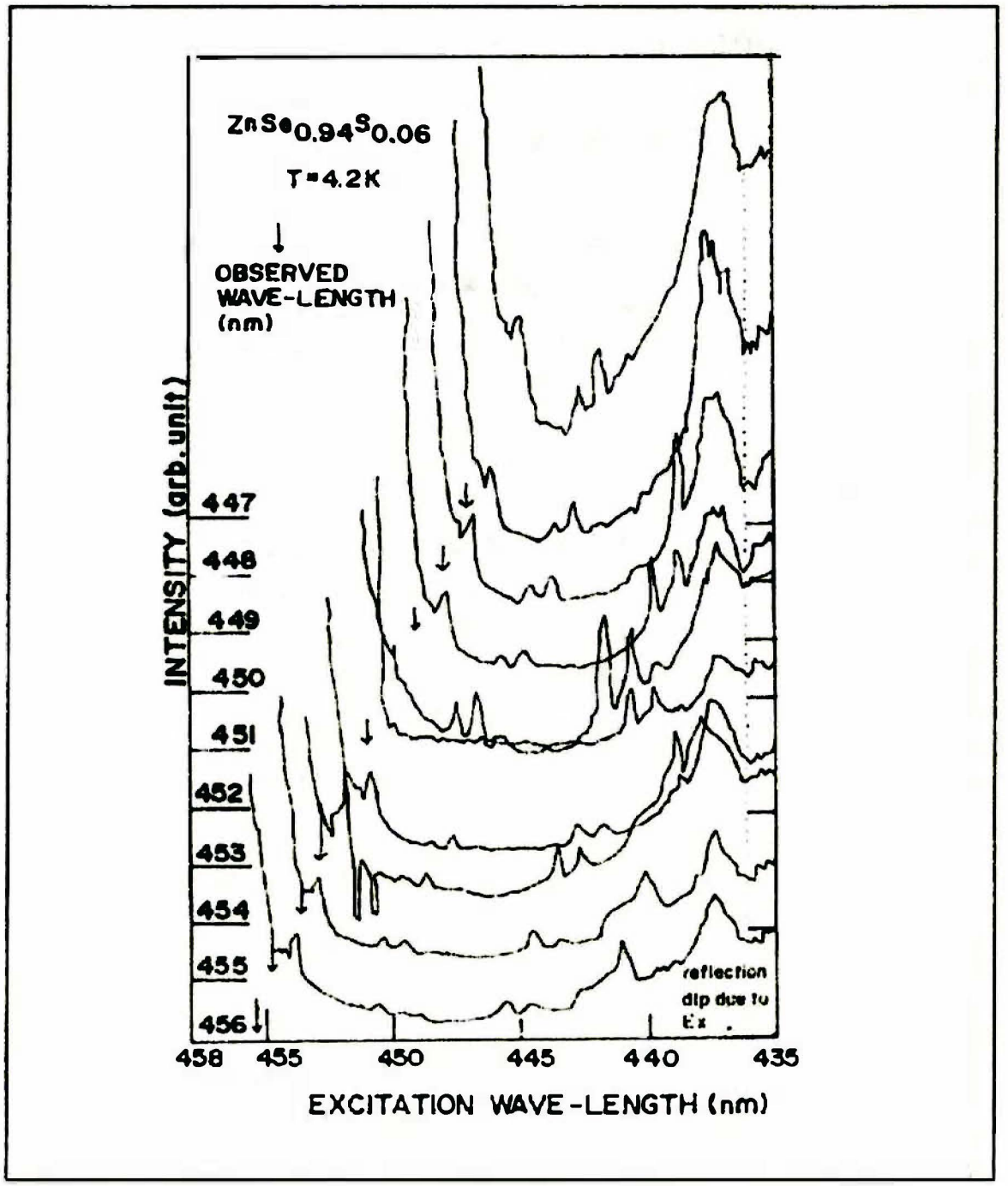

Figure 19. Excitation spectra of the D-A pair band $ZnSe_{0.94}S_{0.06}$ at 4.2 K.

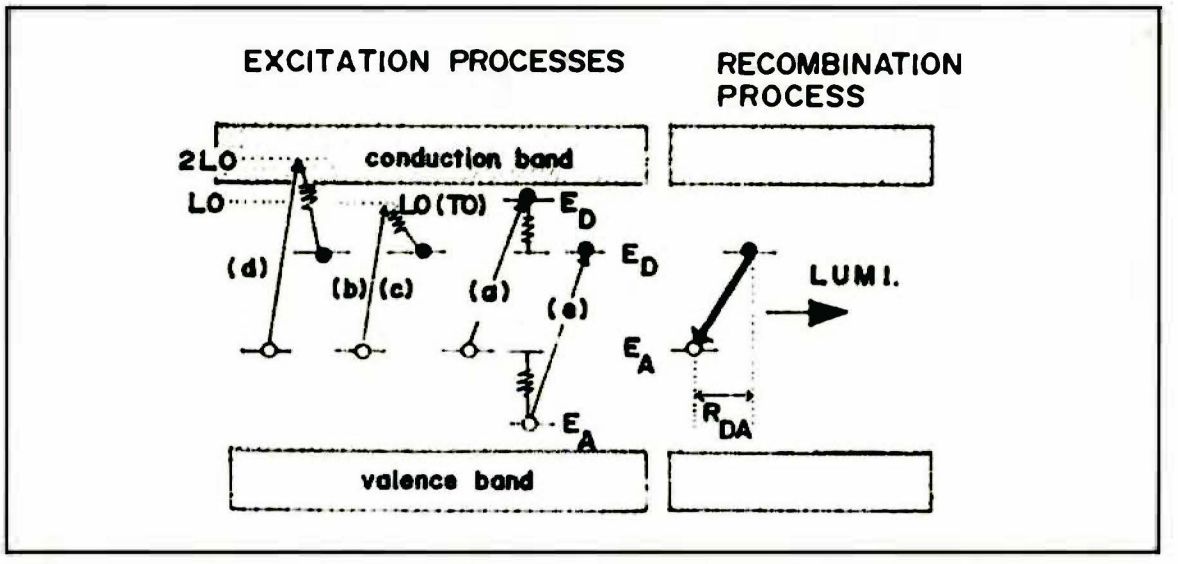

Figure 20. Excitation and recombination processes of donor-acceptor pairs

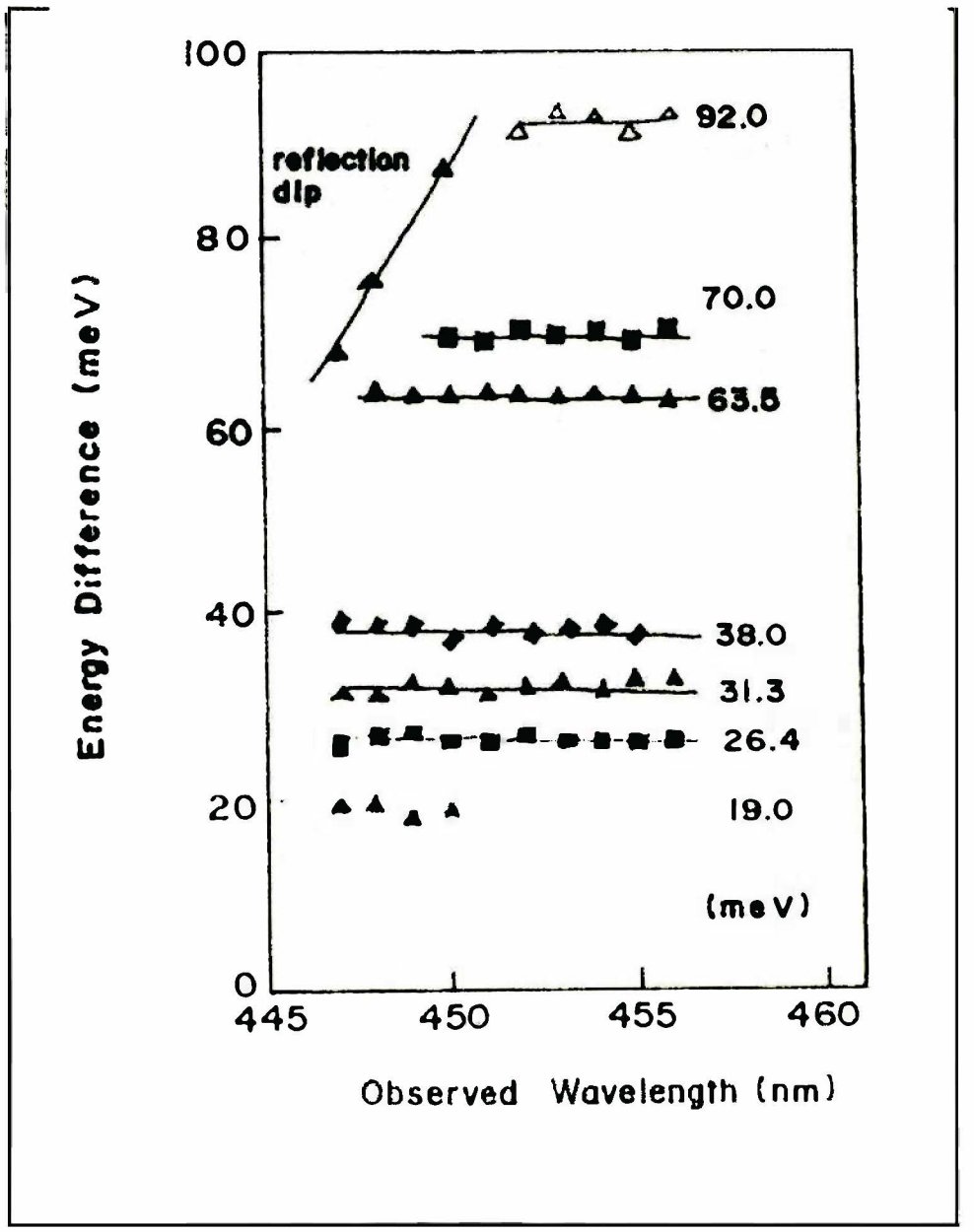

Figure 21. Energy difference ($E_1 - E_e$) vs D-A pair wavelength

at 19.0 meV[(a)] is ascribed to the energy difference between the 1s and 2s states of the donor, which leads to the donor binding energy of E_D-(A1) = 25.5 meV using the hydrogen model. The next two peaks at 26.4 and 31.3 meV [(b) and (c)] correspond to TO and LO phonon energies, respectively. These values are almost the same as those in ZnSe[40]). The peak at 63.5 meV[(d)] is twice the energy of the LO phonon. The peaks that appear at 38.0 and 70.0 meV which are higher than the D-A emission are unknown to this date. The Na acceptor energy is derived as 122.6 meV from the peak [(e)] [E(1s) – E(2s)] = 92.0 meV, if the simple hydrogen relation is applied. This energy is also comparable to the known Na acceptor in ZnSe.[41])

V. MECHANICAL PROPERTIES OF $ZnSe_xS_{1-x}$

Static Calibration Curve

Semiconductor to metal transition are ideal calibration markers on a fixed point pressure scale because associated with the transition is a decrease in electrical resistance of several orders of magnitude that can be easily detected and measured[43]. They provide convenient calibration points for high pressure apparatus where the electrical resistance variation measurement is utilized.

The split-sphere type apparatus as shown in Fig. 22 is originally designed by Kawai[44] at Osaka University. The significant features of the apparatus are as follows: It has the capability to compress a charge of large volume up to very high pressures and this makes it possible to obtain pressures higher than 20 GPa over a volume of about 5 mm^3. Hence, samples of several milligrams are compressed up to pressures higher than 1000°C by using an internal heating system. A pressure environment in the specimen is maintained in a highly hydrostatic state by multi-anvils, which are equivalent to each other in size and in movement, in spite of the use of a solid medium for the pressure transmission. Figure 23 shows a schematic diagram of the multi-anvils.

Sintered MgO is used as the transmitting medium instead of the conventional pyrophyllite since the latter may cause a reduction of the pressure value at high temperatures. Moreover, gaskets are used to produce a hydrostatic environment for the sample. It is a known fact that in ungasketted samples, the region of maximum pressure originates in the central area and decreases radially at the edge of the anvil. There is usually a large pressure distribution across the sample in the ungasketted method. In experiments conducted under nonhydrostatic conditions, the presence of stress gradients and the unknown magnitude of stress often cast serious doubt on the interpretation of the desired measurements. In the gasketted method, these undesirable effects are eliminated. The usage of gaskets also offers the advantage of prolonging the useful lifetimes of the anvils and of allowing maximum pressure to be obtained without anvil failure.

Experimental Procedure and Results

ZnSe and ZnS are known to undergo semiconductor to metallic phase change. Their pressure-induced phase transition points are among those that made up the fixed-point static calibration curve[4-8]. Utilizing the transition pressure of ZnS as obtained by Piermarini, et al.[6] and those of Bi I-II and Bi III-V (as agreed upon in the 1968 International Conference of the National Bureau of Standards), the phase transition points of $ZnSe_xS_{1-x}$ ($0.40 \leq x \leq 1$) are determined wherein the pressure-induced variation of electrical resistance is measured.

In this study, very high pressures are generated within the 6-8 split-sphere vessel with a pressure-transmitting medium which are finally compressed in a 5,000-ton uniaxial press and electrical measurements are subsequently conducted.

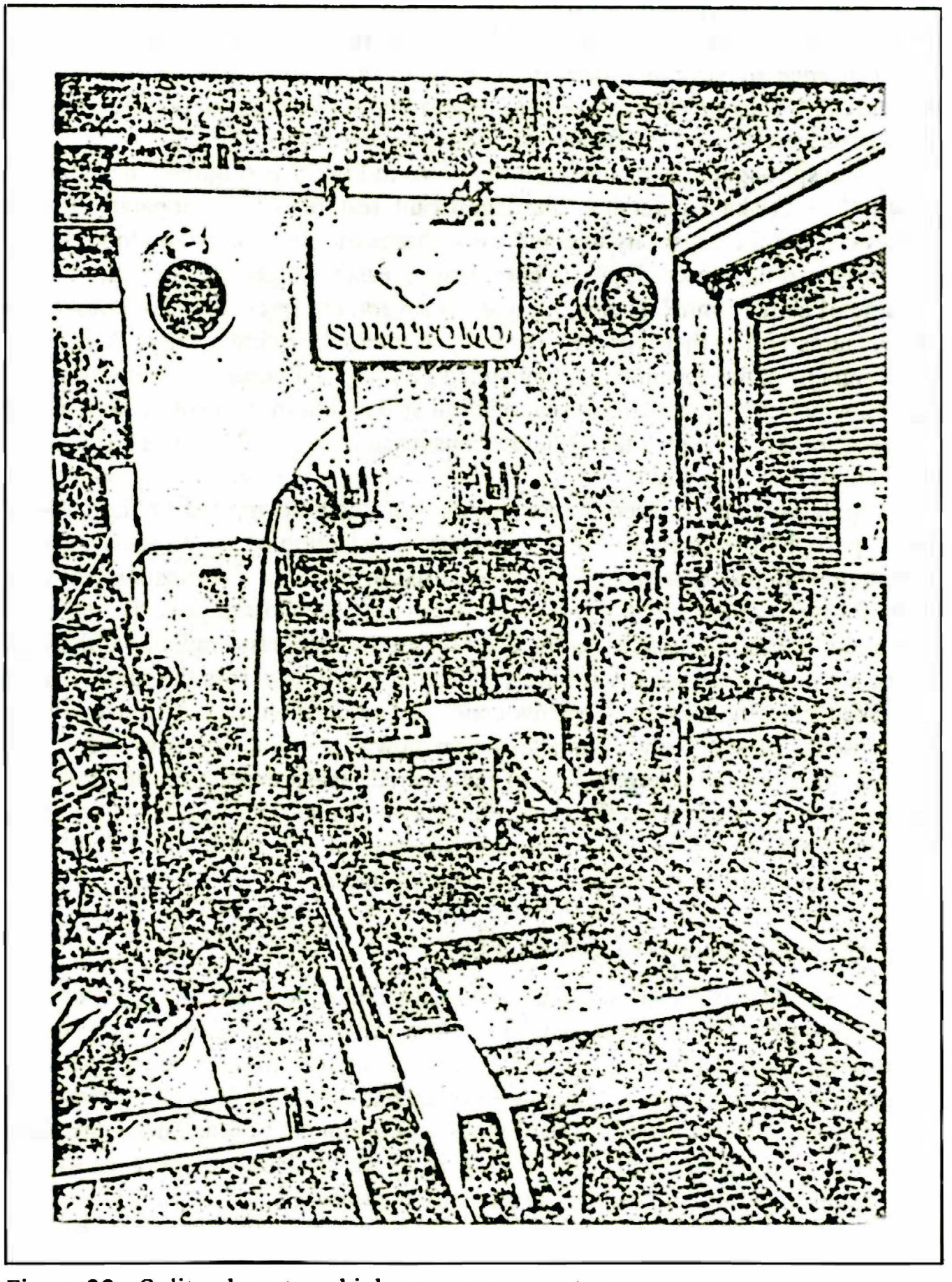

Figure 22. Split-sphere type high pressure apparatus

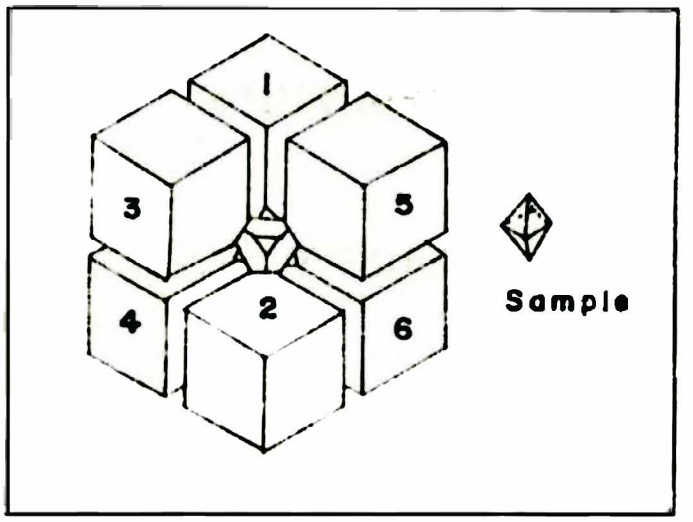

Figure 23. Schematic diagram of multi-anvils

Figure 24 shows a cross section of the octahedral MgO pressure-transmitting medium which is 14 mm to a side. Two to four holes (0.8-mm diam) are drilled through the medium wherein each were inserted with crushed crystallites of the samples and 3.0 ~ 3.1 mm-long, Cu strip-covered pyrophyllite bars acting as electrodes are thrust in from both ends of each hole. The pressure-transmitting medium is then held by a tungsten-carbide cube made of 8 separate anvils insulated from each other by cardboard and fluorine-enriched resined adhesive tape and gaskets made of pyrophyllite are utilized.

The variation of the electrical resistance is observed in the loading stage for most of the samples. From 3 ~ 4 MΩ, the corresponding resistance of ZnSe, $ZnSe_xS_{1-x}$, and ZnS dropped abruptly to about a hundred for ZnSe and $ZnSe_xS_{1-x}$ and a few kΩ for ZnS. Figure 25 shows the behavior of the resistance of $ZnSe_{0.80}S_{0.20}$ with respect to pressure using a 10-mm octahedral MgO as pressure-transmitting medium. In the loading stage, the resistance has a very sluggish increase from 1.95 MU to 2.55 MΩ and falls rapidly when the applied oil pressure is 131 kgf/cm^2; after which, the resistance drop is observed for 10 min. With the pressure released, the resistance does not immediately return to its original value. It is only after one-third of the pressure has been deloaded that resistance starts to increase. After another one-third of the pressure has been released, the resistance returns to its former value at a fast rate where, in fact, its final value is even greater than the initial.

The semiconductor to metallic transition pressure of ZnSe is determined to be 13.0 ⊕ 0.4 GPa using as calibration points the static transformation pressures of Bi I-II, Bi II-V, and ZnS which are 2.550 ⊕ 0.006 GPa, 7.7 ⊕ 0.3 GPa, and 15.0 ⊕ 0.5 GPa, respectively. Employing the transition pressure of ZnSe obtained in this work as fixed point together with the aforementioned calibration points, the phase-transition pressures of $ZnSe_{0.80}S_{0.20}$, $ZnSe_{0.60}S_{0.40}$, $ZnSe_{0.50}S_{0.50}$, and $ZnSe_{0.40}S_{0.60}$ in units of GPa are determined as interpreted from experimental results where oil pressure is measured in kgf/cm^2. Figure 26 shows the pressure-induced phase transition points of $ZnSe_{0.80}S_{0.20}$, $ZnSe_{0.60}$,$S_{0.40}$, $ZnSe_{0.50}S_{0.50}$,

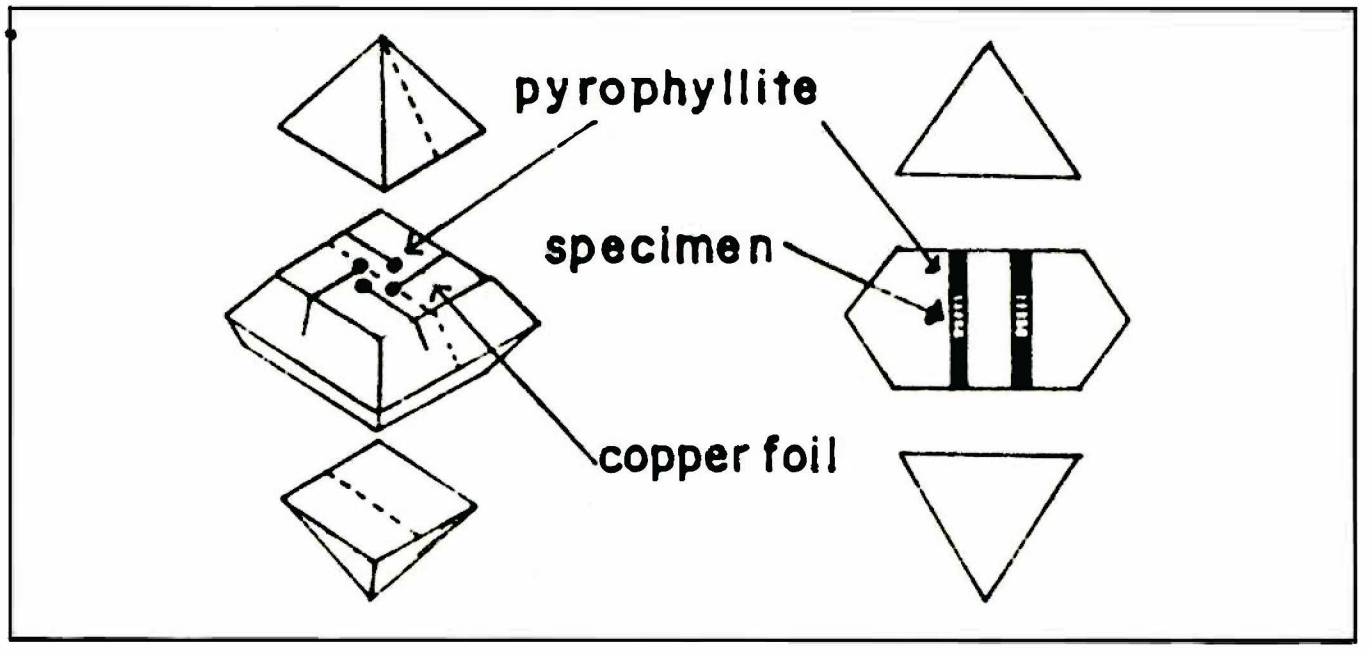

Figure 24. Cross section of the octahedral MgO pressure-transmitting medium

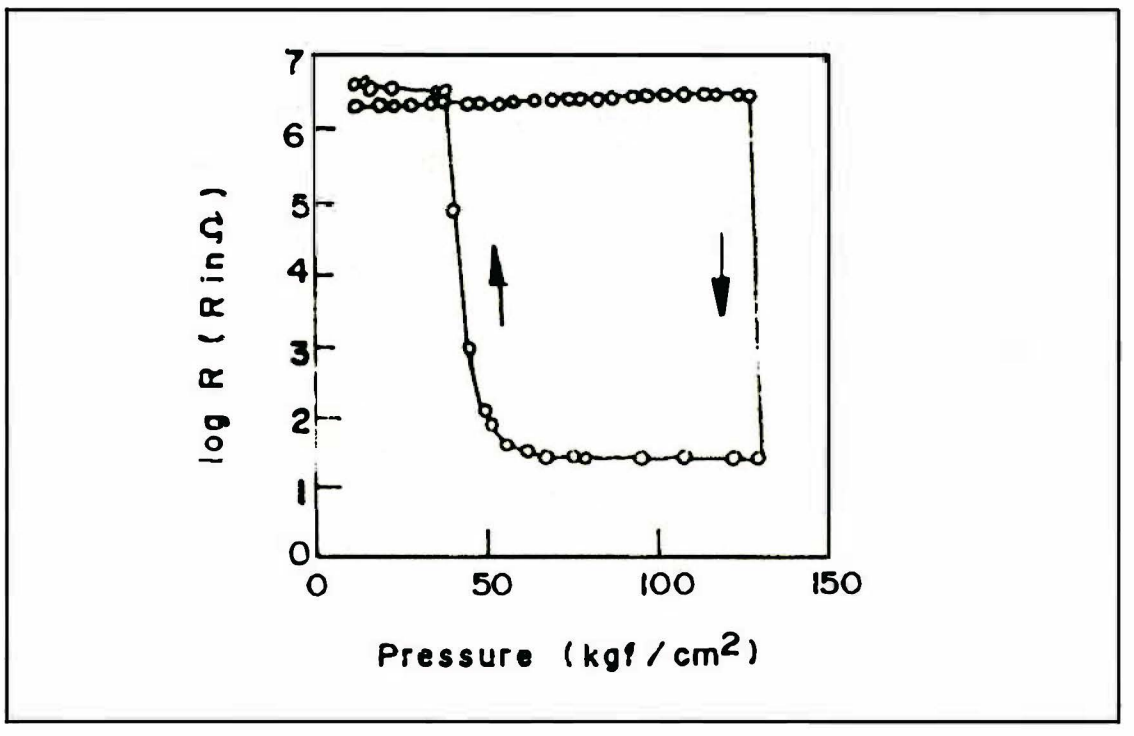

Figure 25. Behavior of resistance with respect to pressure

$ZnZnSe_{0.40},S_{0.60}$, and ZnS, respectively. The transition pressure has an almost linear variation with increasing ZnS composition in $ZnSe_xS_{1-x}$.

Hogoniot Curves of $ZnSe_{0.85},S_{0.15}$

Aside from the measurement of the static transformation pressure, the Hugoniot curves (shock velocity, U_s – particle velocity, u_p, and pressure, P – particle velocity, u_p) of $ZnSe_{0.85},S_{0.15}$, single crystals are determined and the aforementioned curves are compared with those obtained by Gust[27] and Bridgman[45].

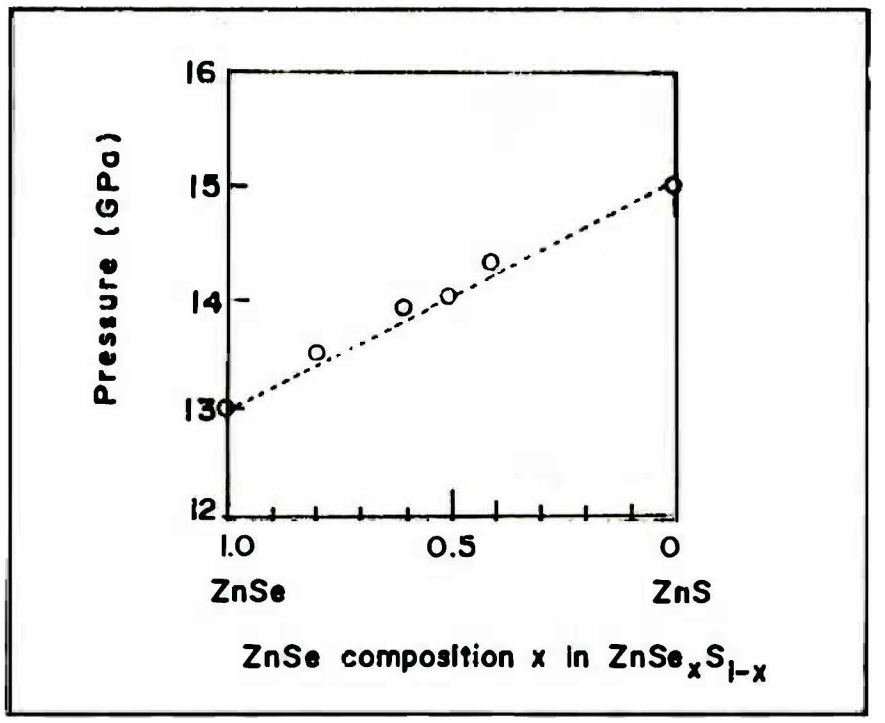

Figure 26. Relationship between static transformation pressure and the ZnSe composition in $ZnSe_xS_{1-x}$

To obtain the shock comptession curve, a single stage powder gun is used. Its schematic diagram is shown in Fig. 27. A sample assembly, as shown in Fig. 28, which employed the pin-contactor method[46] to measure the shock wave velocity through the specimen is used. A test specimen with a size of approximately 5 x 5 x 2 mm[5] is fixed on the rear surface of a 1.0-mm thick copper driver plate. Three tilt pins each of which is equipped with a spring are pressed on 12 μm-thick mylar sheets forming the vertices of a triangle with the specimen at the center. The tilt pins function to determine the inclination or tilt of the shock wavefront in the sample. The end pin which detects the shock wavefront that is propagated through the specimen is pressed on a 12 μm-thick mylar strip and a 15 μm-thick copper strip on top of the center of the rear surface of the specimen. The electric signals from the pins which carry the information of the time required for the propagation of the shock wavefront through the sample and the inclination of the shock wavefront are monitored from the outgoing circuits. The sample is struck by a 2.5 mm-thick copper flyer plate accelerated by a single stage powder gun whereby the impact velocity is measured by the magnet flyer method[47].

The $U_s - u_p$ Hugoniot of the specimen is shown in Fig. 29. In this case, the u_p's are determined by the impedance match method using experimental data on the shock wave velocity and the flyer impact velocity. Normally, the impedance method used in this data analysis produces errors in u_p if a compressed material undergoes plastic deformation or phase transition. Nevertheless, the deviation from the linear relationship may be attributed to the differences among the samples used. The uniform shock wave velocity can be explained by the fact that only the elastic wave velocity can be measured if it is faster than those of the plastic and/or phase transition waves.

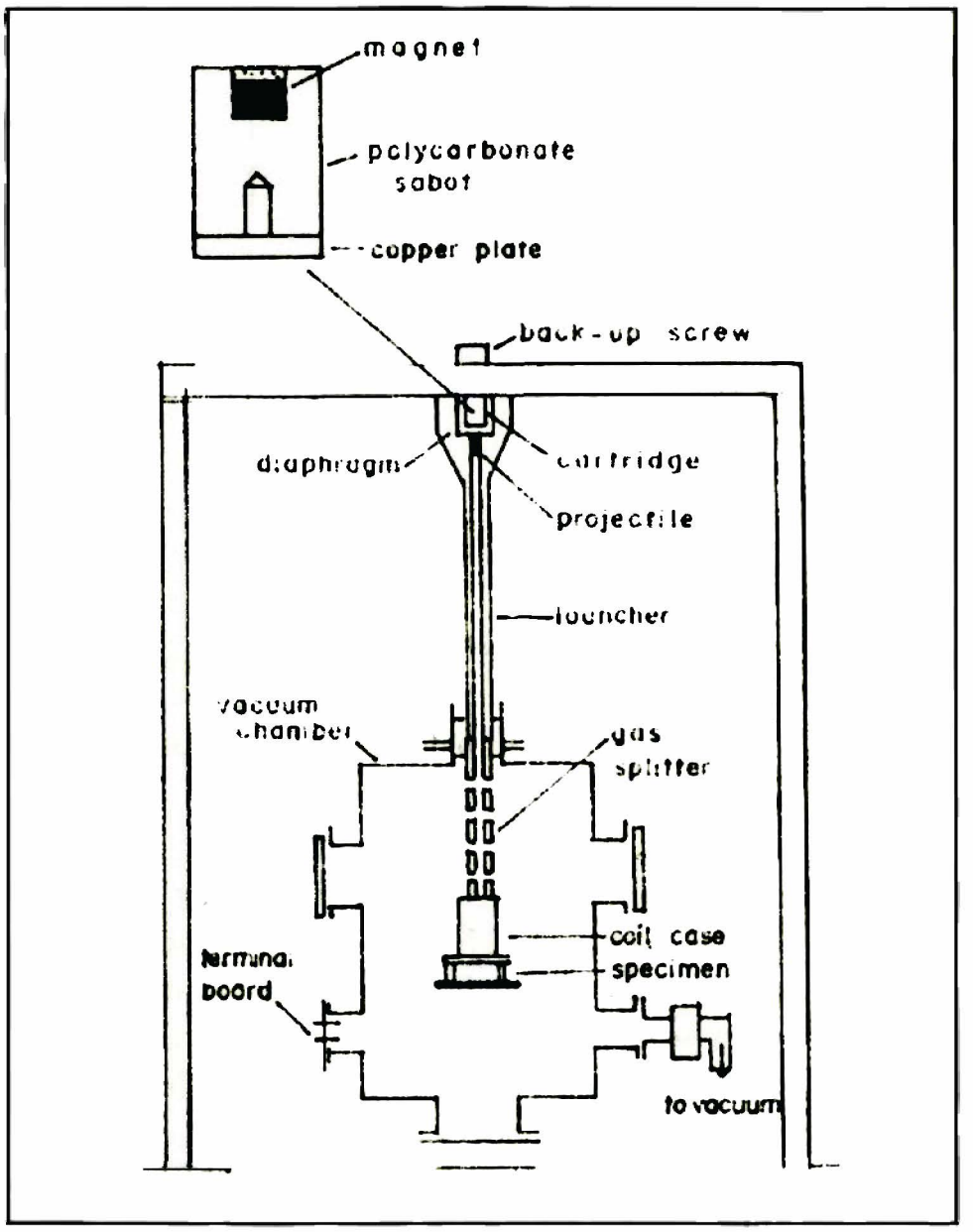

Figure 27. Schematic diagram of a vertical single stage powder gun

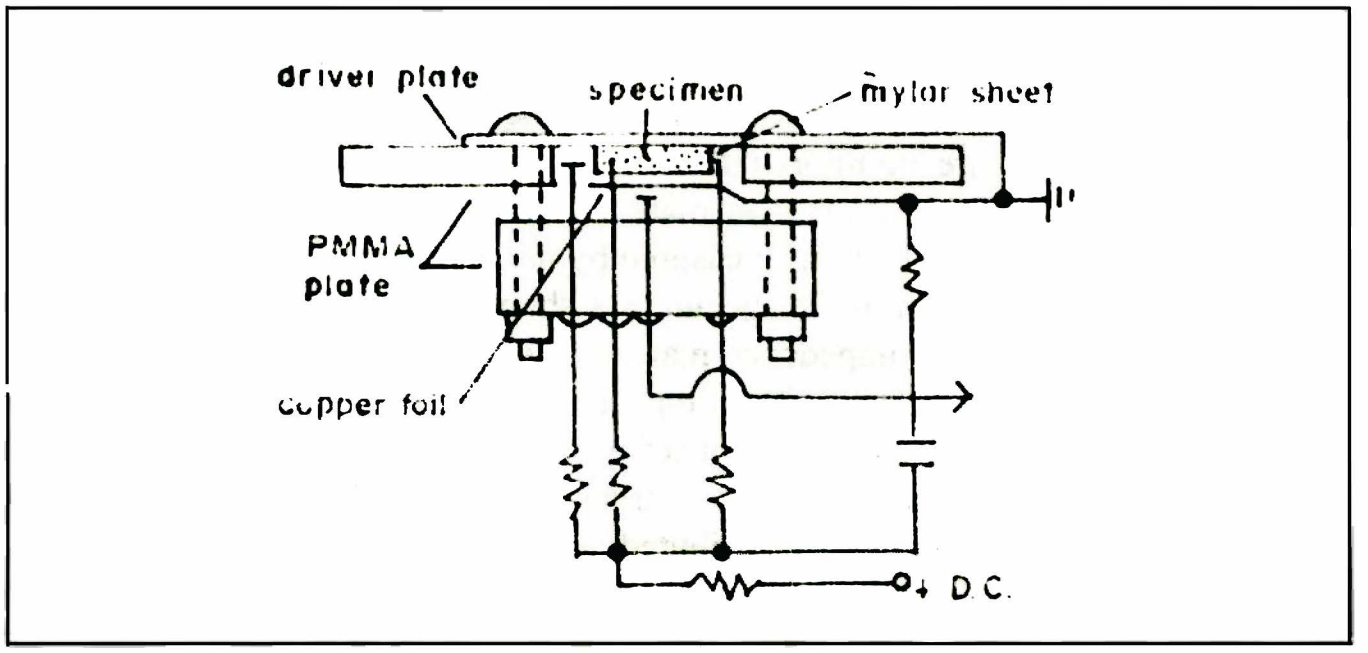

Figure 28. Schematic diagram of a sample assembly for shock wave loading

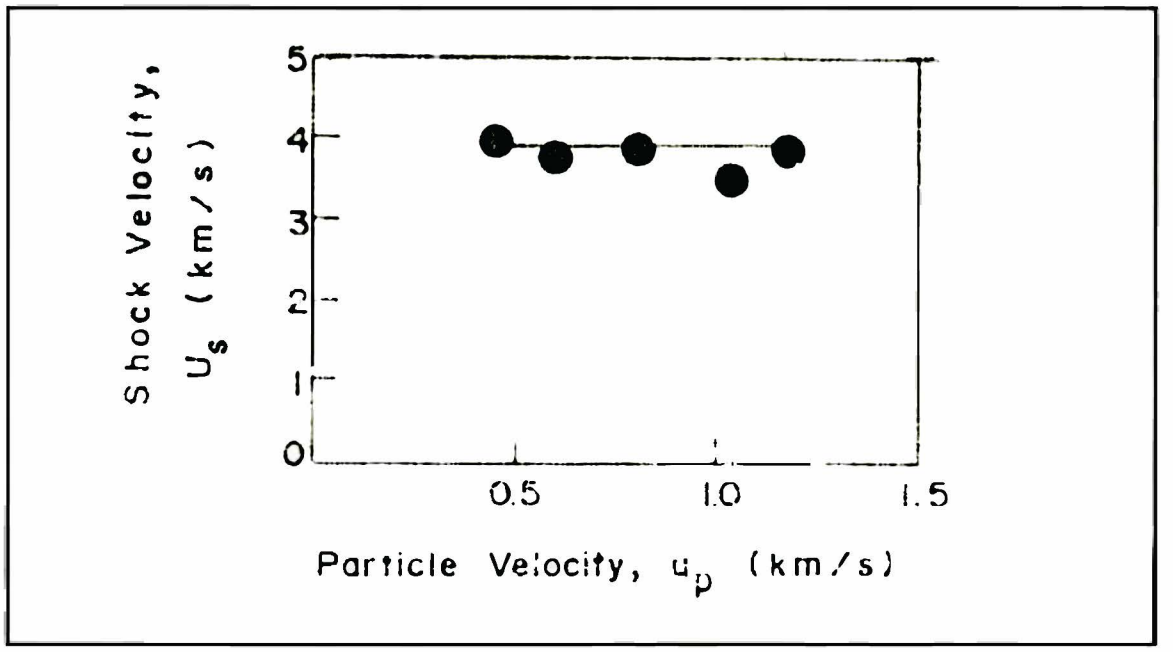

Figure 29. Shock velocity vs. particle velocity of $ZnSe_{0.85}S_{0.15}$

The density, ρ and the pressure, P in the shock-compressed state can be determined by employing the basic equations of shock wave which are derived from mass and momentum conservation laws considering that U_s and u_p are previously known. The initial density of the test specimen is measured to be 5.07 g/cm^3.

The P – u_p Hugoniot translated from the U_s – u_p Hugoniot is shown in Fig. 30. Comparing the experimental results with Gust's data, it can be inferred that the sample may have undergone a phase change. Although the pin-contactor method used in this work can only measure the elastic wave, the data extrapolated agree very well with the corresponding P – u_p Hugoniots of ZnS and ZnSe up to the phase transition point in the first plastic wave region; notwithstanding the fact that the impedance match method used may have produced errors if the sample under consideration has undergone plastic deformation or phase transition. Figure 30 indicates that the errors are very minimal since the experimental curve resolved from the U_s – u_p Hugoniot to a P – V curve (cf. Fig. 31) agrees very well with Bridgman's data. It is however unresolve to take the extrapolated data on the second plastic wave region since this can involve substantial errors.

In order to compare the P – V Hugoniot measured experimentally in this study with those obtained from Bridgman's static pressure data, the isothermal pressure, P for the test specimen is calculated using the following equation which is derived from Gruneisen's equation of state [48]

$$P - P_H = \rho\gamma C_V(T - T_H) \tag{10}$$

where P is the isothermal pressure, P_H is the pressure on the Hugoniot, ρ is the specimen's density, γ is the Gruneisen parameter, C_V is the specific heat at constant volume, T is the room temperature and T_H is the temperature on the Hugoniot. T_H is calculated using the thermodynamic equations[49], viz.:

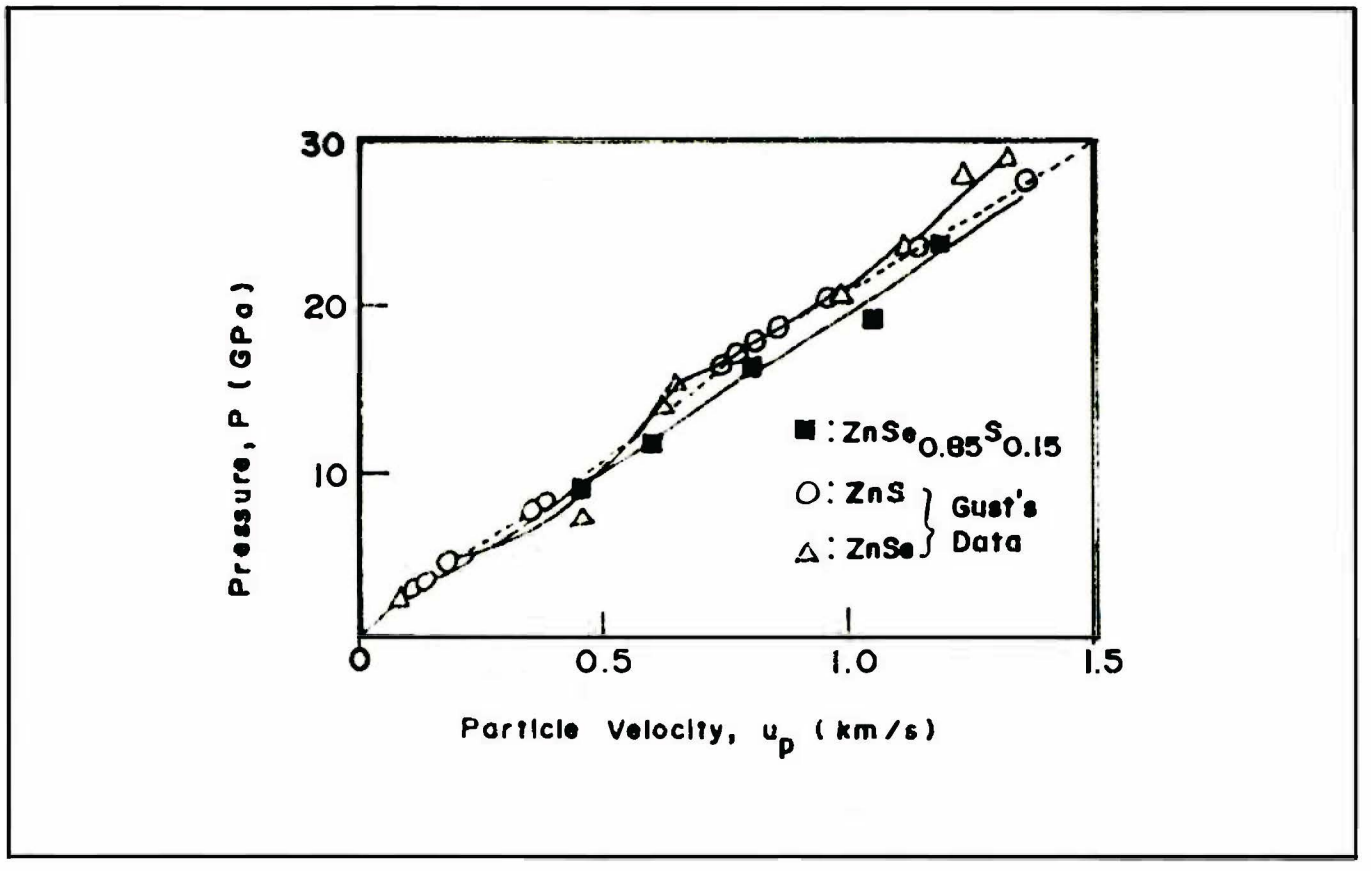

Figure 30. Pressure vs. particle velocity relationship of $ZnSe_{0.85}S_{0.15}$, ZnS, and ZnSe.

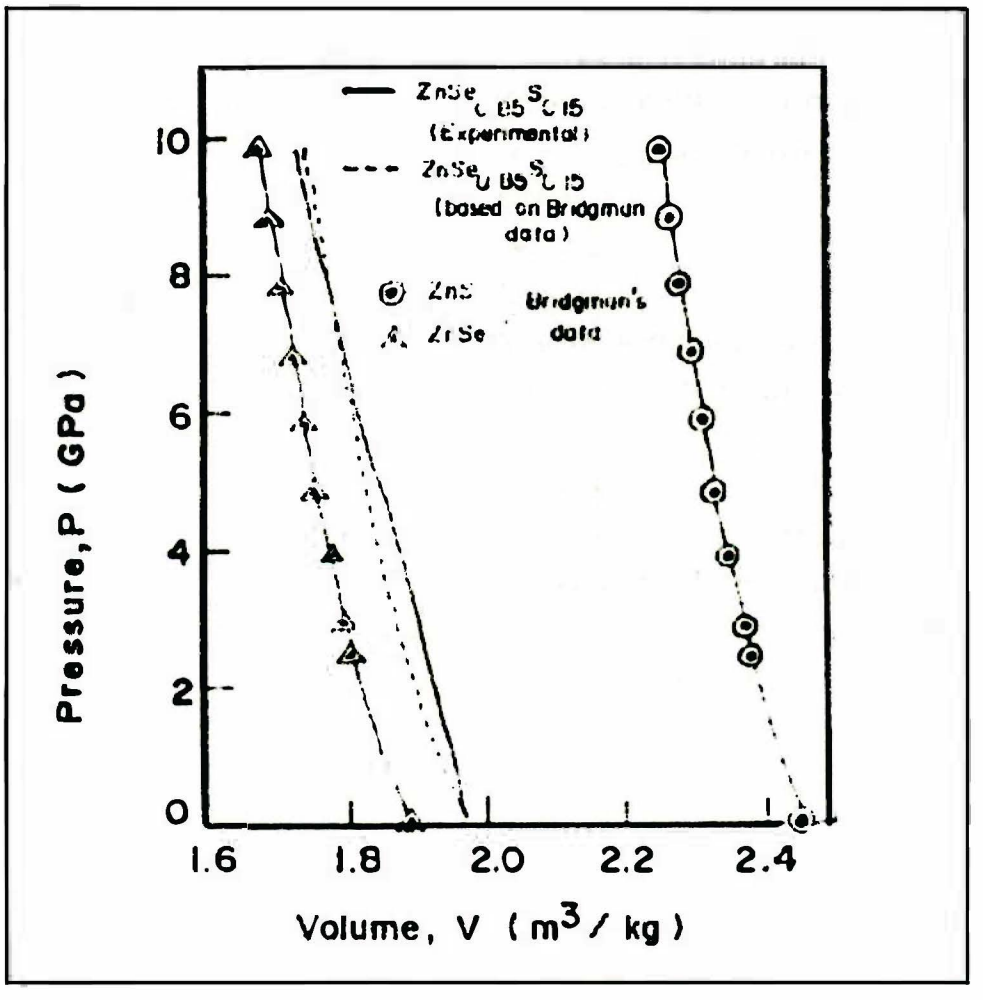

Figure 31. Pressure vs. volume relationship of $ZnSe_{0.85}S_{0.15}$, ZnS. and ZnSe

$$\frac{dT_H}{T_H} = -\gamma \frac{dV}{V} + \frac{dS}{C_V} \tag{11}$$

$$2T_H\, dS = (V_o - V)\, dP + (P - P_o) dV \tag{12}$$

In Eq. (12) dS is solved and substituted in Eq.(11) to obtain the temperature along the Hugoniot. In this work, the product of the Gruneisen parameter, γ and the density, ρ is calculated to be 4.07 g/cm^3 using Soma's[50] data for ZnS and ZnSe. The specific heat at constant volume[51, 52] is calculated to be

$$C_V = (37.39 + 3.80 \times 10^{-3}T - 8.76 \times 10^{4}T^{-2}) \times 105 \text{ (erg/gk)} \tag{13}$$

Figure 31 describes the P-V Hugoniots of ZnS and ZnSe calculated from Bridgman's data. Also shown are the experimental data on $ZnSe_{0.85}S_{0.15}$ which are found to show good fitting to those of $ZnSe_{0.85}S_{0.15}$ based on Bridgman's data using Munson and Schuler's[52] formulation, thus verifying further the validity of the measured data.

Up to the phase transition point, the data obtained in this work are valid since the experimental curve resolved from the Us-up Hugoniot to a P-V curve fits very well with that based on Bridgman's data. Before the phase transition pressure, the P-V Hugoniot of $ZnSe_{0.85}S_{0.15}$ agrees very well with those corresponding to ZnS and ZnSe.

CONCLUSIONS

$ZnSe_xS_{1-x}$ single crystals are grown by means of the self-closed sublimation method at 1250°C in a stream of argon gas for several days where the growth tube is partially open at the start of growth to remove volatile impurities. The grown crystals are almost free from twinning and are well-facetted with either the (111) or (110) planes as depicted by their Laue diffraction patterns. Furthermore, the crystals are found to have a well-pronounced zincblende structure with their respective lattice constants conforming with Vegard's law.

The optical properties of the crystals are analyzed by measuring their photoluminescence as well as their excitation spectra at 4.2 K. The sample crystals are as-grown, annealed in Zn vapor, Na-doped, and Li-doped. The luminescence spectra of the as-grown samples are dominated by the excitonic lines which are the free exciton and the bound exciton lines. Broad band luminescence in the low energy side is seldom observed in the as-grown samples. The I_2 lines are seen at high resolution from very good crystals. These lines are due to the decay of excitons bound to neutral donors. The I_1^{deep} lines show the strongest emission intensity. These lines are due to the decay of excitons bound to neutral acceptors. The I_1^{deep} lines have strong phonon cooperation where the longitudinal optical (LO) phonon energy is 31.3 meV and the transverse optical (TO) phonon energy is estimated to be 26.4 meV for $ZnSe_{0.94}S_{0.06}$.

Some of the crystals are annealed in Zn vapor for 24 hr at about 900°C and it is found that after this treatment, the intensity ratio of I_1 to I_2 (I_1/I_2) drastically falls. It is concluded therefore that the acceptors are Zn vacancies (V_{Zn}) or associated defects containing V_{Zn} since as a result of the decrease in the density of the Zn vacancies after annealing in Zn, the intensity of the I_1^{deep} line decreases. Also, a strong broad band accompanied by LO phonon replicas appears. This broad band is due to the recombination of donor-acceptor pairs as judged from its spectral shape and energy position and verified by the measurement of the excitation spectra of the aforementioned crystal.

Na- or Li-doping decidedly enhances donor-acceptor pair transitions as evidenced by the appearance of the P_o or the Q_o band in the photoluminescence spectra even without subjecting the sample crystal to heat treatment in Zn vapor. Moreover, the emission energy difference between the Q_o and the P_o bands is confirmed to be 13 meV.

The excitation intensity is varied to evaluate the behavior of the donor-acceptor pair band. The Q_o-0LO band of the Li-doped ZnSe shifts by ~ 2.9 meV for every tenfold increase in intensity while that of as-grown $ZnSe_{0.92}S_{0.08}$ shifts by ~ 4.7 meV or the same tenfold increase in intensity. Moreover, the band broadens with increasing excitation intensity. A particular feature found for the Q_o band is that it has a relatively small bandwidth compared with P_o.

The excitation spectra of a donor-acceptor pair band are measured for $ZnSe_{0.94}S_{0.06}$ and the energy differences between the observed donor-acceptor pair and the peak energies are plotted as a function of the observed wavelength of the donor-acceptor pairs. All peaks relative to the observed donor-acceptor pair have correspondingly constant energy separations. The lowest energy peak at 19.0 meV is the energy difference between the 1s and 2s states of the donor. Using the hydrogenic model, the binding energy of the al donor is 25.5 meV and that of the Na acceptor is derived to be 122.6 meV.

Aside from the optical properties, the mechanical properties of $ZnSe_xS_{1-x}$ ($0.40 \leq x \leq 1$) are also evaluated. The high pressure polymorphs of these crystals are analyzed by measuring their respective semiconductor to metal transition points using the electrical variation method.

Very high pressures are generated within the 6-8 split-sphere pressure vessel with a sintered MgO pressure-transmitting medium which are compressed in a 5,000-ton uniaxial press. Electrical measurements are conducted and the resistance drops from several MΩ to about a hundred Ω for ZnSe and $ZnSe_xS_{1-x}$ and a few kΩ for ZnS. The transition pressure for ZnS as obtained by Piermarini, et al. and those of Bi II-II and Bi III-V as determined in the 1968 International Conference of the National Bureau of Standards are utilized and the transition point of ZnSe is determined. Based on the transition point of ZnSe, the transition points of $ZnSe_{0.80}S_{0.20}$, $ZnSe_{0.60}S_{0.40}$, $ZnSe_{0.50}S_{0.50}$, and $ZnSe_{0.40}S_{0.60}$ are experimentally determined and are hereby reported to have a linear variation with increasing ZnS composition in $ZnSe_xS_{1-x}$

The Hugoniot curves of $ZnSe_{0.85}S_{0.15}$ single crystals are also determined and compared with the results of Gust and Bridgman. The pressure-particle velocity Hugoniot implies that the crystal has undergone a phase change and the extrapolated data agree very well with those of ZnSe and ZnS as reported by Gust. The P-V curve resolved from the experimental shock velocity – particle velocity Hugoniot also agrees very well with Bridgman's data. It is concluded then that at very high pressure, $ZnSe_xS_{1-x}$ undergoes a phase change from semiconductor to metallic state.

REFERENCES

1. Y.S. Park and B.K. Shin: in Topics in Applied Physics ed. J. Pankove (Springer, Berlin, 1977) Vol. 17, pp. 133-170.
2. Y. Marfaing: *Prog. Crystal Growth Characterization* 4 (1981) 317.
3. J.L. Pantrat. N. Magnea, and J.P. Faurie: *J. Appl. Phys.* 53 (1982) 8668.
4. A.S. Balchan and H.G. Drickamer: *Rev. Sci. Instrum.* 32(1961) 308.
5. H.G. Drickamer: *Rev. Sci. Instrum.* 41 (1970) 1667.
6. G.J. Piermarini and S. Block: *Rev. Sci. Instrum.* 46(1975) 973.
7. B. Le Niendre, K. Suito, and N.Kawai: *High Temp. and High Pressures* 8 (1976) 1.
8. A.L. Ruoff and K.S. Chan: High Pressure Science and Technology eds. K.D. Timmerhaus and M.S. Barber (Plenum, New York, 1979) Vol. 1, p. 779.
9. P.J. Dean and J.L. Merz: *Phys Rev.* 178 (1969) 1310.
10. J.L. Merz, H. Kukimoto, K. Nassau, and J.W. Shiever: *Phys. Rev.* B6 (1972) 545.
11. P.J. Dean: *Phys Rev.* B4 (1971) 24596.
12. M.D. Ryall and J.W. Allen: *J. Phys. Chem. Solids* 34(1974) 2137.
13. G.E. Hite, D.T.F. Marple, M. Aven, and B. Segall: *Phys. Rev.* 3 (1967) 156.
14. J.C. Bouley, P. Blanconnier, A. Herman, PhGe, P. Henoc and J.P. Noblanc: *J. of Appl. Phys.* 46 (1975) 3549.
15. M. Yamaguchi, A. Yamamoto and M. Kondo: *J. Appl. Physics* 48 (1977) 5237.
16. S. Fujita, H. Mimoto, and T. Noguchi: *J. Appl. Physics* 50 (1979) 1070.
17. P.K. Chatterjee, A.J. Rosa and B.G. Streetman: *J. Lumin.* 8 (1973) 176.
18. A.J. Rosa and B.G. Streetman: *J. Lumin.* 10 (1975) 211.
19. S. Gezci and J. Woods: *J. Lumin.* 10 (1975) 267.
20. F.J. Bryant and P.s. Manning: *J. Phys. Chem. Solids* 35 (1974) 97.
21. V. Swaminathan and L.C. Greene: *Phys Rev.* B14 (1976) 5351.
22. E.F. Gross, S.A. Permogorov and B.S. Razbirin: *J. Phys Chem. Solids* 27 (1966) 1647.
23. B. Segall and G.D. Mahan: *Phys. Rev.* 171 (1968) 935.
24. W.C. Tait and R.L. Weiher: *Phys. Rev.* 178 (1969) 1404.
25. K. Ohmori, M. Ohishi, T. Okuda, and M. Hiramatsu: *J. Appl. Physics* 49 (1978) 4506.
26. M. Ohishi: Japanese *J. of Appl. Physics* 25 (1986) 1546.
27. W.H. Gust: *J. Appl. Physd.* 53 (1982) 7.
28. Yagi and Akimoto: *J. Appl. Phys.* 47 (1976) 3350.
29. D.L. Decker: *J. Appl. Phys.* 37 (1966) 5012.
30. L. Cemik and A. Neuhaus: *High Temp. and High Pressures* 6 (1974) 203.
31. S.L. Bell and S. Sen: *J. Vacuum Sci. Tech.* A3 (1985) 112.
32. W. Gibbs: Collected Works, Thermodynamics (Yale Univ. Press, New Haven, 1968) Vol. 1.
33. F. Pizzarello: *J. Appl. Phys.* 25 (1954) 804.
34. W.W. Piper and S.J. Polich: *J. Appl. Phys.* 32 (1961) 1278.
35. D.C. Reynolds: in The Art and Science of Growing Crystals ed. J.J. Gilman (John Wiley, New York, 1963) p. 62.

36. W.L. Bragg: *Proc. Cambridge Phil. Soc.* 17 (1913) 43.
37. J.L. Merz, K. Nassau, and J.w. Shiever: *Phys. Rev.* B8 (1972) 1444.
38. J.J. Hopfield: *J. Phys Chem. Solids* 10 (1959) 110.
39. R.A. Street and W. Senske: *Phys. Rev. Lett.* 37 (1976) 1292.
40. M. Aven, D. Marple, and B. Segall: *J. Appl. Phys. Suppl.*, 32 (1961) 2261.
41. H. Tews, H. Venghays, and P.J. Dean: *Phys. Rev.* B19 (1970) 5178.
42. E. Gutsche ad O. Geode: *J. Lumin.* 1-2 (1970) 200.
43. S. Block, R.a. Forman, and G.J. Piermarini: in High Pressure Research ed. M.H.Manghnani and S. Akimoto (Academic Press, New York, 1977) p. 503.
44. N. Kawai: in A Static High Pressure Apparatus With Tapering Multipiston Formed A Sphere I, *Proc. Japan Acad.* 42 (1966) pp. 358-388.
45. P.W. Bridgman: *Proc. Am. Acad. Arts & Sci.* 76 (1948) 55.
46. G.E. Duvall and G.R. Fowles: High Pressure Physics and Chemistry (Academic Press, London, 1963) Vol. 2, p. 209.
47. K. Kondo, A Sawaoka and S. Saito: *Rev. Sci Instrum.* 48 (1977) 1581.
48. E. Gruneisen: Handbuch der Physik (Verlag J. Springer, Berlin, 1926) Vol. 10, p. 22.
49. R.G. McQueen, S.P. Marsh, J.W. Taylor, J.N. Fritz, and W.J. Carter: High Velocity Impact Phenomena (Academic Press, New York, 1970) pp. 294-299.
50. T. Soma: *Solid State Com.* 34 (1980) 927.
51. C. Kittel: Introduction to Solid State Physics (John Wiley and Sons, Inc., New York, 1966) 3rd ed., p. 155.
52. II-VI Zoku Kagohbutsu Handohtal Kesshoh Databook (II-VI Group Compounds Semiconductor Crystals Databook, Japanese Electronics Society, Tokyo, 1983) pp. 46-94 in Japanese.
53. D.E. Munson and K.w. Schuler: Proc. 17th Segamore Army Mat. Res. Conf., New York, 1070 (Syracuse Univ. Press, New York, 1971) p. 185.
54. D.G. Thomas, M. Gershenzon and F.A. Trumbore: *Phys. Rev.* A133 (1964) 269.
55. R.E. Halsted and M. Aven: *Phys. Rev. Lett.* 14 (1965) 64.